Exploring HONO production from particulate nitrate photolysis in Chinese representative regions: characteristics, influencing factors and environmental implications

Bowen Li[1], Jian Gao[1], Chun Chen[1], Liang Wen[1], Yuechong Zhang[1], Junling Li[1], Yuzhe Zhang[1], Xiaohui Du[1], Kai Zhang[1], Jiaqi Wang[1]

[1]State Key Laboratory of Environmental Criteria and Risk Assessment, Chinese Research Academy of Environmental Sciences, Beijing 100012, China

Correspondence to: Jiaqi Wang (wang.jiaqi@craes.org.cn), Kai Zhang (zhangkai@craes.org.cn)

Abstract. The production mechanism of atmospheric nitrous acid (HONO), an important precursor of hydroxyl radical (OH), was still controversial. Few studies have explored the effects of particulate nitrate photolysis on HONO sources in different environment conditions across China. In this work, the photolysis rate constants of particulate nitrate for HONO production ($J_{NO_3^- - HONO}$) were determined through photochemical reaction system with $PM_{2.5}$ samples collected from five representative sites in China. We developed a method to correct and quantify the "shadowing effect" — potential light extinction within aerosol layers at heavy $PM_{2.5}$ loadings on the filters — for $J_{NO_3^- - HONO}$ measurements, which showing that elemental carbon (EC), the dominant light-absorbing component in $PM_{2.5}$, played a dominant role in it. The corrected $J_{NO_3^- - HONO}$ values varied with sampling period and location over a wide range, distributing from 1.6×10^{-6} s^{-1} to 1.96×10^{-4} s^{-1}, with a mean ($\pm$ 1 SD) of $(1.71 \pm 2.36) \times 10^{-5}$ s^{-1}. Chemical compositions, specifically nitrate loading and organic component, affected the production of HONO through particulate nitrate photolysis: high $J_{NO_3^- - HONO}$ values were generally associated with the $PM_{2.5}$ samples with high OC/NO_3^- ratio ($R^2 = 0.86$). We suggested that the parameterization equation between $J_{NO_3^- - HONO}$ and OC/NO_3^- established in this work can be used to estimate $J_{NO_3^- - HONO}$ in different aerosol chemical conditions, thus reducing the uncertainty in exploring HONO daytime sources. This study confirms that the photolysis of particulate nitrate can be a potential HONO daytime source in rural or southern urban sites, which are characterized by high proportion of organic matter in $PM_{2.5}$.
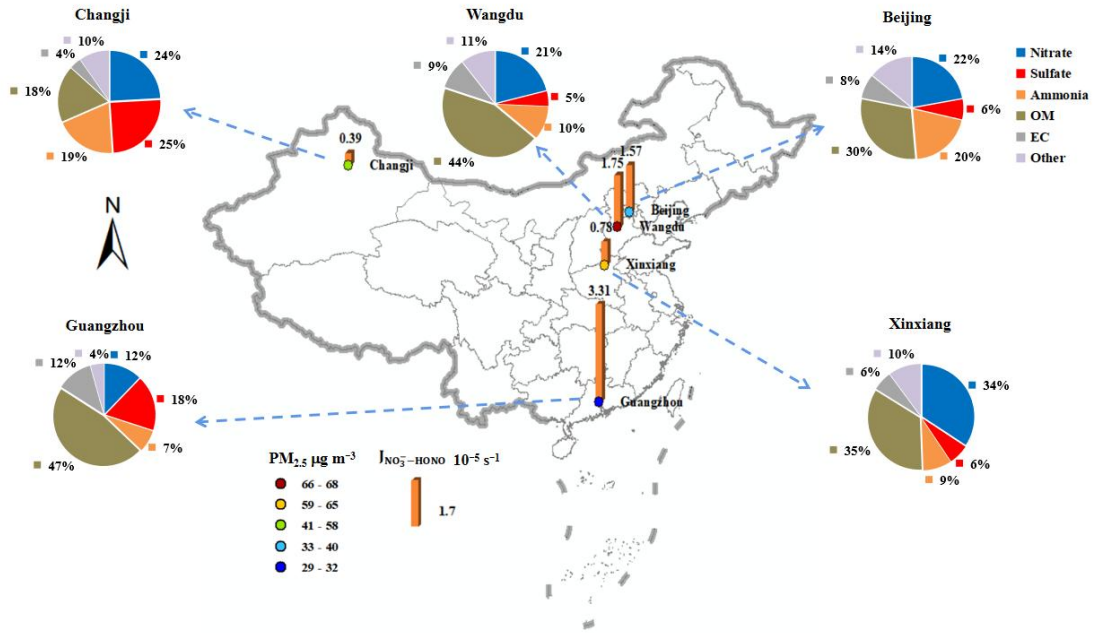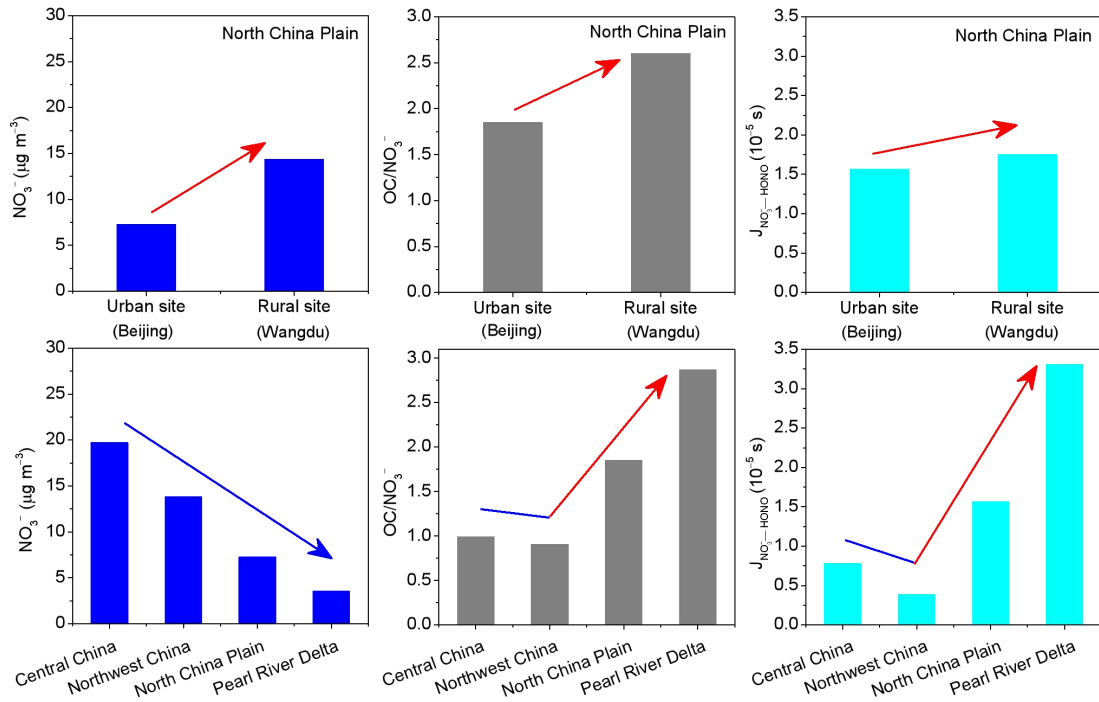
1 Introduction

Gaseous nitrous acid (HONO) is an important nitrogen-containing trace gas in the troposphere, which can produce hydroxyl radical (OH) through photolysis, thus stimulating the enhancement of atmospheric oxidation and the formation of secondary aerosols (Fu et al., 2019; Slater et al., 2020; Ren et al., 2003; Li et al., 2011; Su et al., 2011). In recent years, the contribution of HONO to atmospheric oxidation in heavily polluted conditions has attracted great attention (Villena et al., 2011; Fu et al., 2019; Slater et al., 2020). Even though observational research on HONO has been conducted for nearly 40 years, the understanding of HONO daytime source was still controversial (Fu et al., 2019; Wang et al., 2017; Mora Garcia et al., 2021). Numerous mechanisms have been proposed to explain the extremely high HONO concentrations at noon, including direct combustion emission (Kurtenbach et al., 2001; Liang et al., 2017; Liao et al., 2021), gas-phase reaction of NO and OH radical (Li et al., 2011; Zhang et al., 2016), heterogeneous reaction of NO_2 (Wang et al., 2017; Ammann et al., 1998; Monge et al., 2010; Stemmler et al., 2006), soil emissions (Su et al., 2011; Oswald et al., 2013; Melissa A, 2014; Kim and Or, 2019), and the photolysis of HNO_3/nitrate on aerosol or ground surface (Zhou et al., 2003; Zhou et al., 2011; Ye et al., 2016b; Ye et al., 2016a; Ye et al., 2017).

Particulate nitrate, which was conventionally considered as the ultimate oxidation product of NO_x, can rapidly photolyze and recycle NO_x or HONO back to the gas phase (Andersen et al., 2023; Handley et al., 2007; Beine et al., 2006; Ye et al., 2016a; Ye et al., 2017; Ye et al., 2016b; Gu et al., 2022b), at a rate 10 to 300 times faster than the photolysis rate of gaseous HNO_3 ($\sim 7 \times 10^{-7}$ s^{-1}) under typical tropical noontime conditions (Finlayson-Pitts, 2000). Recently, some field, laboratory and modeling works have proposed that photolysis of particulate nitrate can be an important in situ source of HONO in rural, suburban and urban environments (Ye et al., 2016b; Mora Garcia et al., 2021; Liu et al., 2019; Bao et al., 2018; Wang et al., 2017). Fu et al. (2019) found that the photolysis of HNO_3/nitrate in the atmosphere and deposited on surfaces was the dominant HONO source during noon and afternoon, contributing above 50 % of the simulated HONO. However, there are large discrepancies in estimating the rate constants in the atmosphere (Gen et al., 2022). In New York, Ye et al. (2017) reported that the photolysis rates of particulate nitrate in clean areas were two orders of magnitude higher than that in polluted areas, ranging from 6.2×10^{-6} to 5.0×10^{-4} s^{-1}, with a median of 8.3×10^{-5} s^{-1}. The proposed rate constants of nitrate photolysis based on the aircraft observations over South Korea ranged from 7×10^{-6}

60   to 2.1×10^{-5} s^{-1} (Romer et al., 2018). Shi et al. (2021) derived the rate constant ($< 2 \times 10^{-5}$ s^{-1}) based on

61   chamber experiments, but found a limited role of this mechanism to HONO production. The

62   uncertainty of HONO production rate from the photolysis of particulate nitrate can reach up to 1.4 ppbv

63   h^{-1}, and greatly affect the accuracy of HONO source analysis (Liu et al., 2019; Lee et al., 2016; Ye et

64   al., 2016a). The highly-varied photolysis rate constant of particulate nitrate was closely associated with

65   environmental conditions and the aerosol chemical or physical characteristics, such as relative humidity

66   (RH), aerosol acidity, light intensity, and coexisting components (organic components, halogen, etc.)

67   (Gelencsér et al., 2003; Ye et al., 2016a; Bao et al., 2020; Wang et al., 2021; Reeser et al., 2013).

68   Elucidating the mechanism and dominant factors controlling the photolysis of particulate nitrate is

69   important to accurately estimate the HONO production rates from nitrate photolysis, thus improving

70   estimations of HONO budgets.

71   In general, the photolysis rate constant of particulate nitrate was derived though photochemical

72   experiments using bulk particle samples collected on filters (Ye et al., 2017; Bao et al., 2018).

73   Comparing with the suspended particles in the ambient atmosphere, the collected $PM_{2.5}$ particles in the

74   aerosol filters may present a multiple-layer structure, especially in heavy air pollution conditions (Bao

75   et al., 2018). The light-absorbing species within $PM_{2.5}$ particles would hinder the light absorption of

76   particulate nitrate in the lower layers of the filter sample, thus inhibiting the photolysis of particulate

77   nitrate, which was called the "shadowing effect" (Ye et al., 2017). The shadowing effect may be

78   negligible in clean air conditions but should be evaluated and quantified in heavy haze conditions.

79   However, previous works generally ignored this shadowing effect.

80   According to previous field observations, the $PM_{2.5}$ chemical composition, especially particulate

81   nitrate (NO_3^-), showed obvious spatial differences across China (Wang et al., 2022a, b; Wang et al.,

82   2022c; Wang et al., 2016; Cheng et al., 2024). As one of the key industrial development areas in China,

83   the Pearl River Delta Region (PRD) has a great number of large-scale industrial parks dominated by the

84   chemical industry, resulting in significant VOC emissions and a large proportion of organic matter (OM)

85   in $PM_{2.5}$. In the North China Plain (NCP), the particulate nitrate (NO_3^-) has surpassed sulfate (SO_4^{2-})

86   and OM to become the dominant $PM_{2.5}$ component in recent years (Wang et al., 2022b). For now, the

87   investigation of particulate nitrate photolysis in different atmospheric environments was limited in

88   China, and the influence of aerosol chemical or physical characteristics on HONO production was still

89   unclear. In this work, to shed light on the contribution of particulate nitrate photolysis to the HONO

90 daytime source, we examined the photolysis rate constant for HONO based on photochemical

91 experiments with PM$_{2.5}$ samples collected from five typical sites in China. In addition, the shadowing

92 effect due to increasing aerosol particle loading on the filters was quantified. After correcting this effect,

93 the influence of various environmental conditions, including particulate nitrate, organic matter, and

94 aerosol acidity, on the formation of HONO was investigated and the possible role of this photolytic

95 process as HONO sources was also examined.

96 **2 Method**

97 **2.1 Sampling and filter treatment**

98   The ambient PM$_{2.5}$ was collected on Teflon or quartz filters in autumn-winter seasons in five

99 representative sites, i.e., Beijing, Wangdu, Xinxiang, Guangzhou, and Changji, which were shown in

100 Figure 1a and described in detail in the Supporting Information. These cities were located in the North

101 China Plain (NCP, urban: Beijing, rural: Wangdu), Central China, Pearl River Delta Region (PRD), and

102 Northwestern China, respectively. The sampling flow rates ranged from 16.7 to 1050 L min^{-1}, the

103 sampling times from 9 h to 23 h, and the overall sampling volumes of air from 8 m^3 to 1450 m^3, to

104 collect a very wide range of particulate nitrate loadings. The comparison experiments between Teflon

105 and quartz filters have been conducted, and no significant differences in HONO production rates from

106 particulate nitrate photolysis have been found (T<0.01). The sampling settings employed in Wangdu

107 were designed to quantify the shadowing effect (Figure 1b). In Wangdu, PM$_{2.5}$ was collected at a flow

108 rate of 16.7 L min $^{-1}$ with four channels (A, B, C, and D). A and B channels were set for

109 daytime(8:00−17:00) and nighttime (18:00−7:00) PM$_{2.5}$ samples, respectively, and the other two

110 channels were for the "all-day" (including 8:00−17:00 and 18:00−7:00) PM$_{2.5}$ samples. A total of 158

111 effective PM$_{2.5}$ samples were obtained in this study. These aerosol filter samples were labeled and

112 stored at −20°C in the freezer.

113   Fractions with given surface area from each filter sample were used to perform photochemical

114 reaction experiments and analysis of aerosol chemical components. For each PM$_{2.5}$ sample, the fraction

115 with given surface area was rinsed by deionized water and then sonicated for 15 min. The amounts of

116 water-soluble ions including Na$^+$, NH$_4^+$, K$^+$, Mg^{2+}, Ca^{2+}, Cl$^-$, NO$_3^-$, and SO$_4^{2-}$ were measured by ion

117 chromatography (IC, Thermo ICS-2100). To measure the values of carbon components, including

118   organic carbon (OC) and elemental carbon (EC), a part (0.5024 cm^2) of each filter was detected using a

119   thermal optical carbon analyzer (DRI model 2015). The concentration of OM was obtained by

120   multiplying the OC concentration by a factor of 1.6 (Li et al., 2021). $PM_{2.5}$ concentration was estimated

121   by the sum of all the water-soluble ions and carbon components. The surface concentration of $PM_{2.5}$

122   and its components on aerosol filters were calculated through dividing the absorbed loading with the

123   geometric area of the aerosol filter sample ($\mu g\ cm^{-2}$).
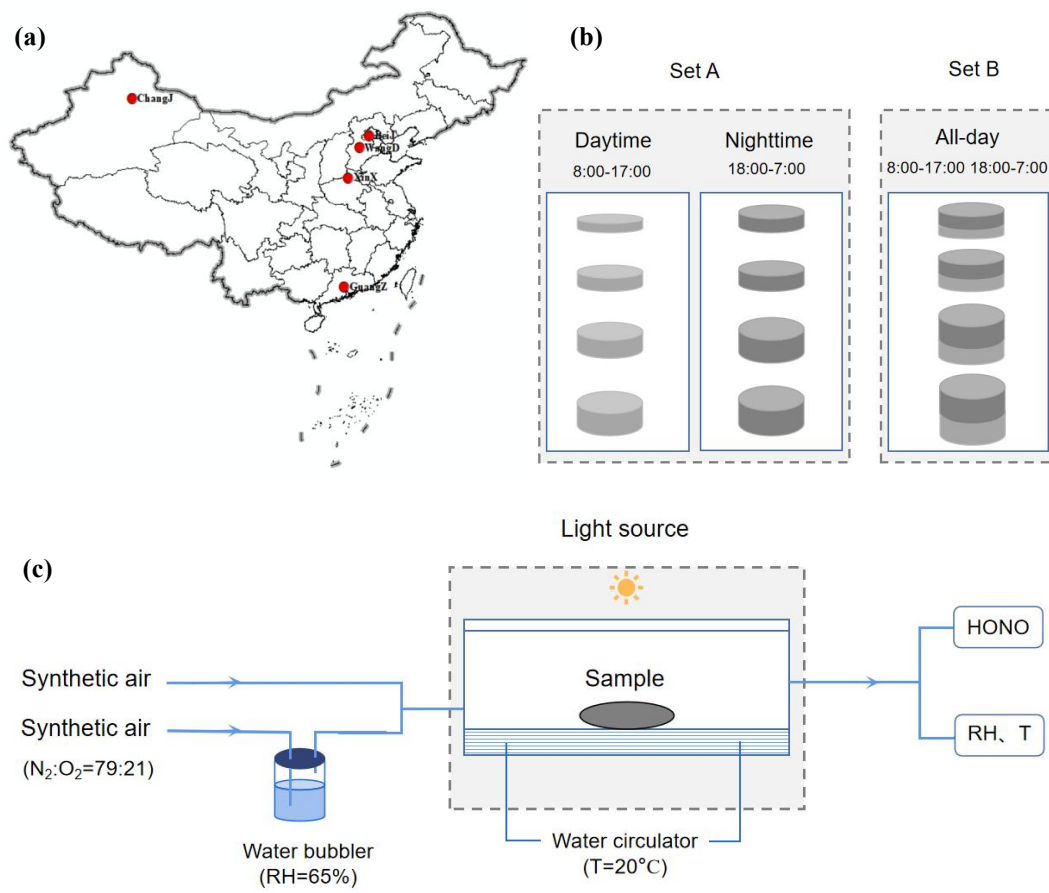
124

125

126   **Figure 1.** (a) Location map of five representative sampling sites in China, (b) the sampling settings to

127   quantify the shadowing effect in Wangdu, and (c) a schematic diagram of the photochemical

128   experimental setup.

129   **2.2 Photochemical reaction system**

130   A custom-made cylindrical quartz vessel was used as the photochemical flow reactor (Figure 1c).

131   The diameter was 10 cm and the depth was 2.5 cm, with a cell volume of ~200 ml. A xenon lamp (300

132   W) was placed 20 cm above the reactor as the light source. The light was filtered by a Pyrex sleeve to

133   remove heat-generating infrared light. The effective light intensity in the center of the flow reactor,

134   where aerosol samples were placed, was measured to be about 0.5 times higher (1.5 kW m^{-2}, measured

135   by a calibrated optical power meter) than that at tropical noon on the ground (solar elevation angle

136     $\theta=0°$). Synthetic air, composed of ultrahigh-purity nitrogen and ultrahigh-purity oxygen mixed at a

137   ratio of 79:21, was used as the carrier gas. The relative humidity (RH) in the air flow was adjusted

138   through a water bubbler and monitored with an online RH sensor (Vaisala, HMT130). The aerosol filter

139   sample was exposed to the solar simulator radiation for 20 min. The photochemical reaction

140   experiment for each sample was repeated 2−3 times with different fractions from the same sample. The

141   gaseous product (i.e., HONO) released during the experiment was flushed out of the reactor by the

142   carrier gas and was detected online by a custom-built HONO analyzer, which had been applied in

143   several measurements previously (Zhang et al., 2020b; Li et al., 2021).

144   **2.3 HONO Production from the photolysis of particulate nitrate**

145   The production rates (nmol h^{-1}) of HONO from particulate nitrate photolysis (P_{HONO}) were

146   calculated from their time-integrated signals above the baselines over the period of light exposure:

147     $$P_{HONO} = \frac{F_g \times 60}{V_m(t_2-t_1)} \int_{t_1}^{t_2} C_{HONO} dt \qquad (1)$$

148   Where F_g (L min^{-1}) is the flow rate of the carrier gas, V_m (24.5 L mol^{-1}) is the molar volume of gas at

149   25 °C and 1 atm of pressure; t_1 and t_2 (min) are the starting and ending time of the irradiation,

150   respectively; C_{HONO} (ppb) is the online measured concentration of HONO. With the flow rate of 2.5 L

151   min^{-1}, the residence time in the reaction system was around ~5 s. The photolytic loss of HONO was

152   less than 5 %, thus no correction was made in the calculation of HONO production.

153   The photolysis rate constant of particulate nitrate leading to HONO production ($J_{NO_3^--HONO}$, s^{-1})

154   was calculated by the following equation:

155     $$J_{NO_3^--HONO} = \frac{P_{HONO}}{N_{NO_3^-} \times 3600} \qquad (2)$$

156   Where $N_{NO_3^-}$ (mol) is the amount of NO$_3^-$ in the tested PM$_{2.5}$ sample. In principle, the photolysis rate

157   constant should be calculated on the amount of NO$_3^-$ that is reachable to the irradiation. However, the

158   amount of the light-reachable NO$_3^-$ in the PM$_{2.5}$ sample was hard to quantify. In this work, the

159   deviation of $J_{NO_3^--HONO}$ due to the overestimate of the amount of NO$_3^-$ under light irradiation, which

160   was called the shadowing effect, would be corrected in Sect. 3.1.

3 Results

3.1 Quantify the influence of the shadowing effect
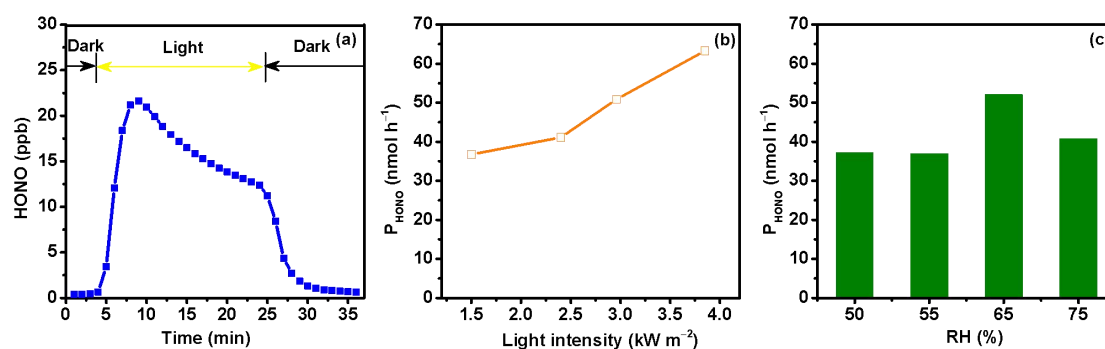
Figure 2. (a) Online measured concentrations of HONO during the light-exposure of an aerosol sample collected on June 12, 2023 in Beijing, P_{HONO} as a function of (b) light intensity (kW m^{-2}) and (c) RH (%).

HONO production within the first 20 min of irradiation during the photochemical experiment was investigated on the PM$_{2.5}$ samples collected from five typical sites in China. Figure 2a showed a typical profile of the changes in HONO concentration in the reaction system. When the light was turned on, HONO concentration in the reactor increased immediately, then leveled off and slightly decayed afterwards. After the light was turned off, the HONO generation stopped immediately and the signal nearly returned to the baseline level. Previous works have revealed that the decay of HONO generation during light exposure period was not resulted from the evaporation loss of particulate nitrate (Ye et al., 2017), but mainly related to the inhomogeneity of particulate nitrate photochemical reactivity or the consumption of reactive electron donors (Bao et al., 2018). HONO production from the photochemical reactions of particulate nitrate were significantly influenced by ambient environmental conditions (i.e., light intensity and RH). As shown in Figure 2b, with the increase of light intensity, P_{HONO} gradually increased, with P_{HONO} in 3.85 kW m^{-2} approximately twice than that in 1.50 kW m^{-2}. Previous works found that the formation of HONO was negligible at low RH (<5%), and increased at intermediate RH (15%−75%), then turned to decrease at RH > 90% (Bao et al., 2018) . Here, we found that P_{HONO} climbed to its highest when RH was around 65 % (Figure 2c). In this work, the photochemical reactions on different aerosol samples were all conducted under the same environmental condition (RH=65 %, temperature=20 °C, and light intensity=1.50 kW m^{-2}).
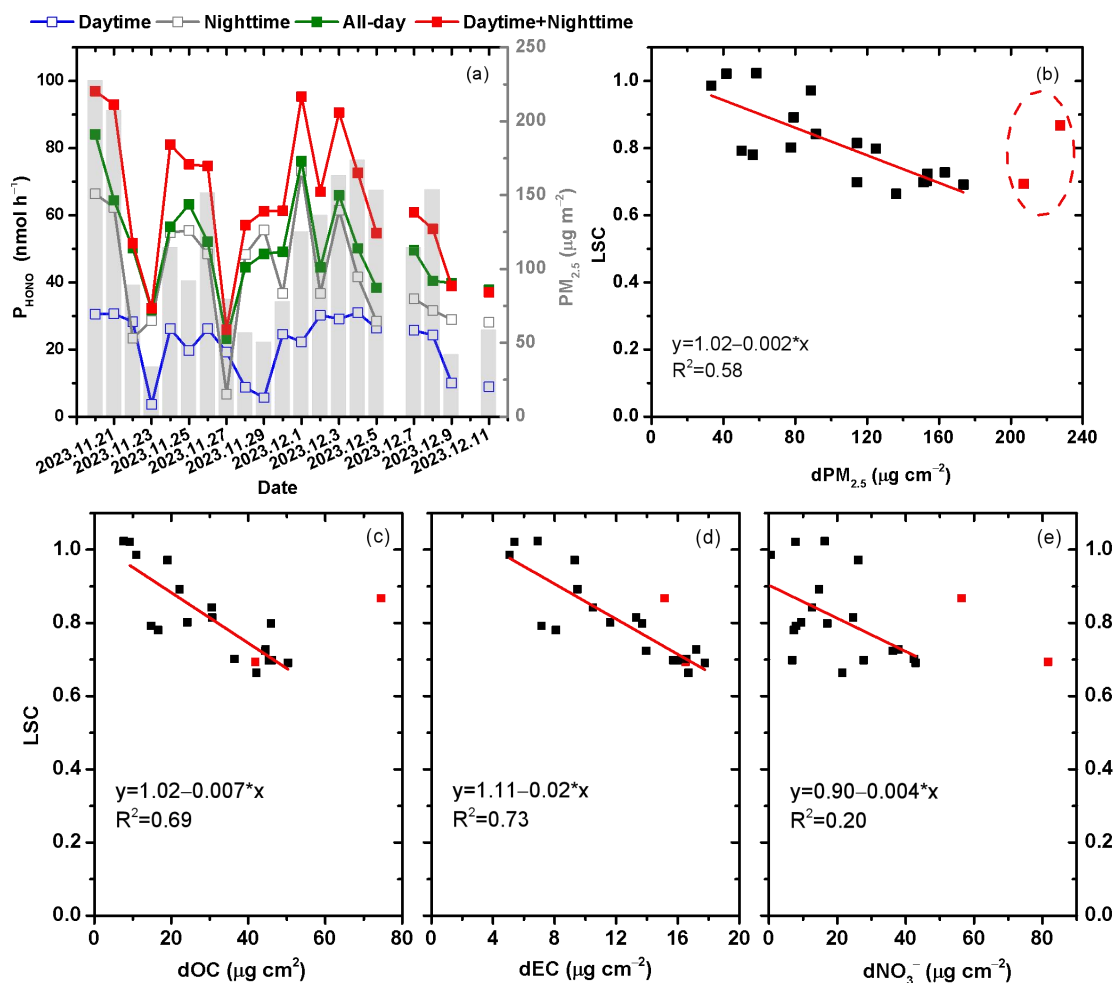
Figure 3. (a) Temporal variation of P_{HONO} for aerosol filters collected in Wangdu during daytime, nighttime and all-day from November 20, 2023 to December 11, 2023, (b)-(e) relationships between light screening coefficient (LSC) and the surface concentrations of $PM_{2.5}$ ($dPM_{2.5}$), OC (dOC), EC (dEC) and NO_3^- (dNO_3^-), respectively. The red squares represent the aerosol samples with $PM_{2.5}$ surface concentration higher than 200 μg cm^{-2}.

As expected, P_{HONO} increased with particulate nitrate loadings in different sampling locations (Figure S1), however, it's interesting to note that, P_{HONO} did not increase or somewhat decreased at very high NO_3^- loading condition. Previous works considered this may be attributed to the shadowing effect, wherein the particulate nitrate underneath the aerosol filters may receive less UV light at heavy aerosol particle loading on the filters, inhibiting the photolysis of particulate nitrate (Ye et al., 2017). Thus, the reported P_{HONO} values for the aerosol filters collected under polluted ambient conditions would be underestimated with heavy aerosol particle loading. To verify and quantify the underestimation of P_{HONO} due to the shadowing effect, we collected two sets of filters in Wangdu (set A: daytime and nighttime, set B: all-day, Figure 1b). Theoretically, the all-day one should share the same NO_3^- loading

200   and chemical composition as the sum of the daytime and nighttime filters, thus the sum of P_{HONO} during

201   daytime ($P_{daytime}^{HONO}$) and nighttime ($P_{nighttime}^{HONO}$) should be equal to that during all-day ($P_{all-day}^{HONO}$) without

202   considering the shadowing effect. A total of 20 pairs of comparative photochemical experiments were

203   conducted, and the comparison of P_{HONO} between these two sets of filters was shown in Figure 3a. We

204   found that the discrepancy between $P_{all-day}^{HONO}$ and $P_{daytime}^{HONO} + P_{nighttime}^{HONO}$ was widening along with the

205   increase of surface $PM_{2.5}$ concentration. To quantify the shadowing effect, we introduced a parameter

206   called "light screening coefficient" (LSC) to describe the decreasing efficiency of light penetrating into

207   the particle with increasing $PM_{2.5}$ loadings:

208   $P_{theory}^{HONO} = P_{daytime}^{HONO} + P_{nighttime}^{HONO}$ (3)

209   $LSC = P_{observed}^{HONO} / P_{corrected}^{HONO} = P_{all-day}^{HONO} / P_{theory}^{HONO}$ (4)

210   where $P_{observed}^{HONO}$ represented the observed production rate of HONO from particulate nitrate photolysis

211   through photochemical experiment, and $P_{corrected}^{HONO}$ represented the corrected value of P_{HONO} after

212   quantifying the shadowing effect. As shown in Figure 3b, when $PM_{2.5}$ surface concentration ($dPM_{2.5}$)

213   was low, LSC was almost equal to 1, indicating that the shadowing effect was negligible. With the

214   increase of $PM_{2.5}$ loading, the value of LSC declined to lower than 65 %. In general, significant

215   negative correlation exited between LSC and $dPM_{2.5}$, except when $dPM_{2.5}$ was higher than 200 $\mu g\ cm^{-2}$

216   (Figure 3b). In this experiment, we assumed that the daytime and nighttime $PM_{2.5}$ samples were both

217   single-layered. However, with the increase of air pollution, these filters in each pair of comparative

218   experiments may already have exhibited the shadowing effect, thus the sum of $P_{daytime}^{HONO}$ and $P_{nighttime}^{HONO}$

219   would be underestimated. Therefore, when quantifying the shadowing effect, the LSC data with $PM_{2.5}$

220   loading higher than 200 $\mu g\ cm^{-2}$ was excluded. Correlations between LSC and the surface

221   concentrations of $PM_{2.5}$ major chemical components, such as EC (dEC), OC (dOC), and NO_3^- (dNO_3^-),

222   were conducted (Figure 3c-e). Significant correlation was found between LSC and carbonaceous

223   component, especially EC ($R^2=0.73$), which was one of the most important light absorbing species in

224   $PM_{2.5}$, indicating that the shadowing effect was mainly related to the light absorption components in

225   $PM_{2.5}$. The relationship between LSC and dEC was established as following:

226   dEC > 5.5 $\mu g\ m^{-2}$: LSC = 1.11−0.02×dEC

227   dEC ≤ 5.5 $\mu g\ m^{-2}$: LSC = 1   (5)

228   when dEC ≤ 5.5 $\mu g\ m^{-2}$, the shadowing effect can be ignored; when dEC > 5.5 $\mu g\ m^{-2}$, P_{HONO} can be

229   corrected by the observed P_{HONO} and LSC, which was estimated using this fitting equation with dEC.

230 Previous works found that the heavy loads of carbonaceous particles can turn these filters into dark

231 brown colors. The UV light was unlikely to transmit efficiently through the dark layer to the particulate

232 nitrate underneath, thus inhibiting the generation of HONO from the photolysis of particulate nitrate

233 (Ye et al., 2017). In consideration of the potential shadowing effect for the daytime and nighttime filters

234 in each pair of comparative experiments, the $P_{daytime}^{HONO}$ and $P_{nighttime}^{HONO}$ observed would be

235 underestimated, and the uncertainty of LSC should be considered at high $PM_{2.5}$ loadings. To evaluate

236 this uncertainty, the observed $P_{daytime}^{HONO}$ and $P_{nighttime}^{HONO}$ values were recalculated and corrected to the

237 theoretical single-layered condition based on Eq. (4) and (5). As shown in Figure S2, with the increase

238 of $PM_{2.5}$ surface concentration, the deviations between LSC and the corrected one have enlarged.

239 However, it's noted that the deviation was still lower than 20 % when $PM_{2.5}$ surface concentration was

240 around 200 μg cm^{-2}. For example, for the aerosol sample collected in December 4, 2023, in Wangdu,

241 the $PM_{2.5}$ surface concentration was 173.57 μg cm^{-2}, and the deviation was 15.74 %, which was

242 acceptable in this work.

243 **3.2 Spatial distribution and temporal variation of HONO production from particulate nitrate**
244 **photolysis**
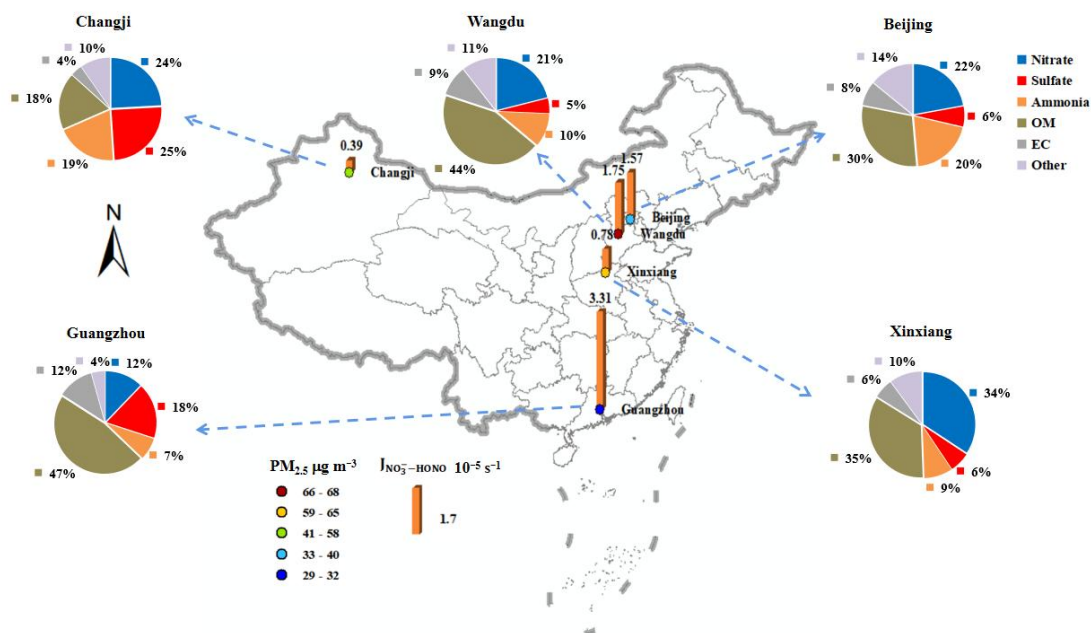
245

246 **Figure 4.** Spatial distribution of the average ($J_{NO_3^- - HONO}$, $PM_{2.5}$ loading, and chemical composition of

247 the aerosol filters collected from five representative cities in China during the observation period.

248   There were 158 filter samples collected from five representative cities in China, and the averaged

249 concentrations of $PM_{2.5}$ and its chemical composition of these filters showed significant spatial

250   characteristics as shown in Figure 4. During the sampling period, OM was the most abundant species in

251     $PM_{2.5}$ over most regions, except in the northwestern city (Changji), and NO_3^- was the dominant

252   inorganic component in the NCP (Beijing and Wangdu) and Central China (Xinxiang), while SO_4^{2-}

253   showed the highest contribution in the PRD (Guangzhou) and Northwestern China (Changji). The

254   values of $J_{NO_3^--HONO}$ on these $PM_{2.5}$ samples were calculated by Eq. (2) with the P_{HONO} corrected by

255   Eq. (4) and (5), and summarized in Figure 4 and Table 1. The corrected $J_{NO_3^--HONO}$, median and mean

256   ($\pm$ one standard deviation), were 1.55×10^{-5} s^{-1} and 1.57 (±2.14) $\times10^{-5}$ s^{-1} in Beijing, 1.68×10^{-5} s^{-1} and

257   1.75 (±2.83) $\times10^{-5}$ s^{-1} in Wangdu, 0.69×10^{-5} s^{-1} and 0.78 (±0.48) $\times10^{-5}$ s^{-1} in Xinxiang, 3.04×10^{-5} s^{-1}

258   and 3.31 (±1.15) $\times10^{-5}$ s^{-1} in Guangzhou, and 0.38×10^{-5} s^{-1} and 0.39 (±0.25) $\times10^{-5}$ s^{-1} in Changji,

259   respectively. The maximum $J_{NO_3^--HONO}$ in these cities ranged from 0.91×10^{-5} s^{-1} in Changji to

260   1.96×10^{-4} s^{-1} in Wangdu. These values were in the comparable range to those previously reported for

261   aerosol samples, such as 1.22×10^{-5} $s^{-1}\sim 4.84\times10^{-4}$ s^{-1} in China by Bao et al. (2018) (RH = 60%,

262   temperature = 25°C, irradiation time=15 min) and 6.2×10^{-6} to 5.0×10^{-4} s^{-1} (the sum of HONO and

263   NOx production, with an average HONO/NOx production ratio of ~2) in US by Ye et al. (2017) (RH =

264   50%, temperature = 20($\pm$1)°C, irradiation time=10 min). It's interesting to note that the average

265     $J_{NO_3^--HONO}$ was the highest in Guangzhou, which was characterized with the lowest $PM_{2.5}$ and NO_3^-

266   concentration among these cities. As for other cities with high $PM_{2.5}$ concentrations, such as Changji

267   and Xinxiang, the corrected $J_{NO_3^--HONO}$ was comparatively lower. According to the National Ambient

268   Air Quality Standard of China (GB3095-2012), the daily $PM_{2.5}$ averages in Guangzhou can meet the

269   Level II standard of 75 $\mu g\,m^{-3}$, while exceeding the level I standard (35 $\mu g\,m^{-3}$). Here, we defined

270     $PM_{2.5}$ polluted days with daily mean $PM_{2.5}$ exceeding 35 $\mu g\,m^{-3}$. As shown in Figure 5, the distribution

271   of the corrected $J_{NO_3^--HONO}$ values in clean days were generally more dispersed and higher than those

272   in polluted days, except in Guangzhou. The average value of $J_{NO_3^--HONO}$ in Guangzhou during air

273   polluted conditions was slightly higher than that in clean conditions, besides much higher than the

274   values in other cities. Because the influence of the shadowing effect has been corrected to some degree,

275   these spatial and temporal change characteristics of $J_{NO_3^--HONO}$ in this work should be mainly related to

276   the varied chemical and physical properties of $PM_{2.5}$ samples collected from different atmospheric

277   environments.

278   **Table 1.** The concentrations of $PM_{2.5}$, NO_3^-, and OC, OC/NO_3^-, corrected $J_{NO_3^--HONO}$, and S_{HONO} in

279   five representative cities in China under different air conditions during the sampling period.

Site	Air condition	PM$_{2.5}$ (µg m^{-3})	NO$_3^-$ (µg m^{-3})	OC (µg m^{-3})	OC/NO$_3^-$	Corrected J$_{NO_3^--HONO}$ (10^{-5} s^{-1}) [a]	S$_{HONO}$ (10^{-5} mol h^{-1} m^{-2}) [b]	S$_{HONO}$ (ppbv h^{-1}) [c]
Beijing	Clean	19.71±8.65	3.15±2.34	3.89±2.13	2.25±3.03	2.01±2.44	0.15±0.07	0.03±0.02
	Polluted	72.56±23.78	19.71±10.72	12.62±2.18	0.87±0.62	0.61±0.30	0.38±0.11	0.09±0.02
	Whole-Min	4.32	0.08	1.07	0.32	0.21	0.04	0.01
	Whole-Max	102.64	32.90	15.95	12.82	11.06	0.57	0.13
	Whole-Mean	32.92	7.29	6.07	1.85	1.57	0.22	0.05
Changji	Clean	20.39±6.00	3.05±1.75	3.61±1.08	1.66±1.11	0.65±0.18	0.07±0.03	0.02±0.01
	Polluted	80.49±39.54	20.59±4.74	8.35±2.97	0.44±0.08	0.21±0.03	0.16±0.04	0.04±0.01
	Whole-Min	14.45	0.88	2.69	0.28	0.16	0.03[d]	0.01[d]
	Whole-Max	169.35	28.28	14.34	3.65	0.91	0.22	0.05
	Whole-Mean	57.37	13.84	6.53	0.91	0.39	0.13	0.03
Guangzhou	Clean	25.62±6.08	3.29±1.68	6.89±2.21	2.72±1.79	3.25±1.28	0.36±0.15	0.08±0.03
	Polluted	40.32±2.23	4.38±1.30	13.82±1.34	3.35±0.86	3.53±0.61	0.59±0.15	0.13±0.03
	Whole-Min	14.77	0.85	3.67	0.82	1.37	0.17	0.04
	Whole-Max	42.74	6.63	15.62	8.05	5.83	0.75	0.17
	Whole-Mean	29.12	3.55	8.54	2.87	3.31	0.41	0.09
Wangdu	Clean	22.16±7.66	3.29±2.59	5.36±2.38	4.79±6.46	3.80±5.10	0.20±0.09	0.04±0.02
	Polluted	83.53±30.47	18.06±12.48	23.23±9.62	1.88±1.67	1.09±0.87	0.50±0.15	0.11±0.03
	Whole-Min	10.67	0.24	2.72	0.22	0.23	0.06	0.01
	Whole-Max	173.45	60.28	63.07	22.06	19.60	0.88[e]	0.20[e]
	Whole-Mean	68.38	14.41	18.82	2.60	1.75	0.42	0.10
Xinxiang	Clean	23.53±5.45	4.35±1.41	5.69±2.46	1.37±0.61	1.28±0.49	0.21±0.07	0.05±0.02
	Polluted	68.98±33.43	24.87±21.5	14.63±4.41	0.87±0.45	0.62±0.35	0.40±0.12	0.09±0.03
	Whole-Min	18.32	2.37	2.33	0.30	0.19	0.09	0.02
	Whole-Max	143.10	73.47	22.06	2.02	1.96	0.59	0.13
	Whole-Mean	57.62	19.74	12.40	0.99	0.78	0.35	0.08

280   [a] represented the photolysis rate constant of particulate nitrate leading to HONO production after considering the

281   influence of the shadowing effect. [b, c] represented the noontime source strength of HONO through the photolysis of

282   particulate nitrate with the units of 10^{-5} mol h^{-1} m^{-2} and ppbv h^{-1}, respectively.[d, e] represented the minimum and

283   maximum values of S$_{HONO}$ during the observation period.
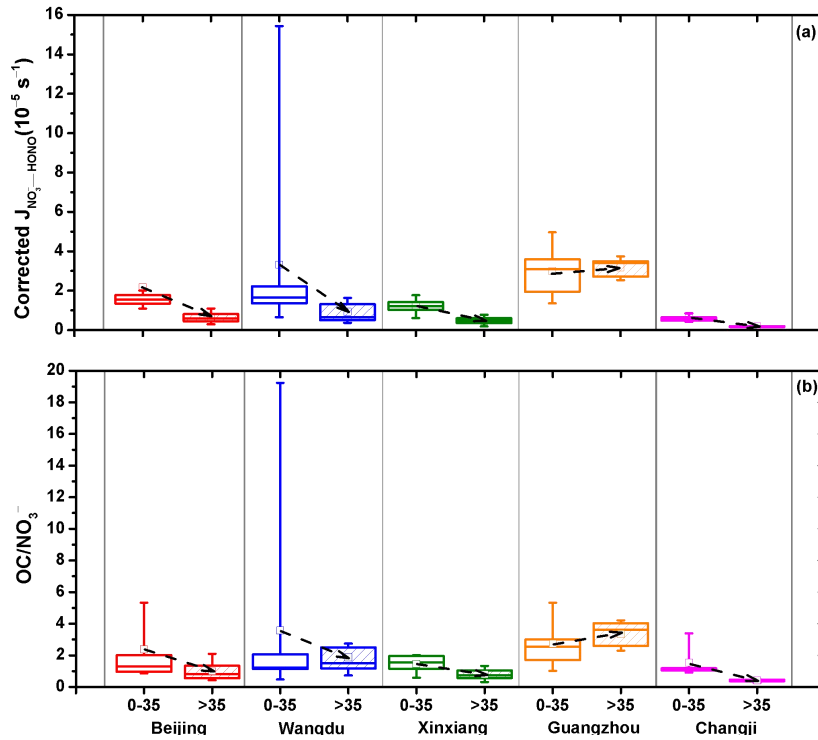
Figure 5. (a) Average corrected $J_{NO_3^- - HONO}$, and (b) the ratio of OC to NO_3^- under different air conditions in five representative cities. The box represents the 25th to 75th percentiles, the horizon line represents the median, the hollow square represents the mean, and the 10th and the 90th percentiles are the bottom and top whiskers, respectively.

3.3 Dominant factors controlling $J_{NO_3^- - HONO}$

3.3.1 Particulate nitrate

As shown in Table 1, the corrected $J_{NO_3^- - HONO}$ values varied with sampling periods and locations over a wide range, distributing from 0.16×10^{-5} s^{-1} for the aerosol sample collected in Changji with $PM_{2.5}$ higher than 90 µg m^{-3}, to 19.60×10^{-5} s^{-1} for the aerosol sample collected in Wangdu with $PM_{2.5}$ lower than 25 µg m^{-3}. Several factors may contribute to the discrepancy of $J_{NO_3^- - HONO}$ in these different aerosol samples, such as particulate nitrate, organic matter, and aerosol acidity.

298
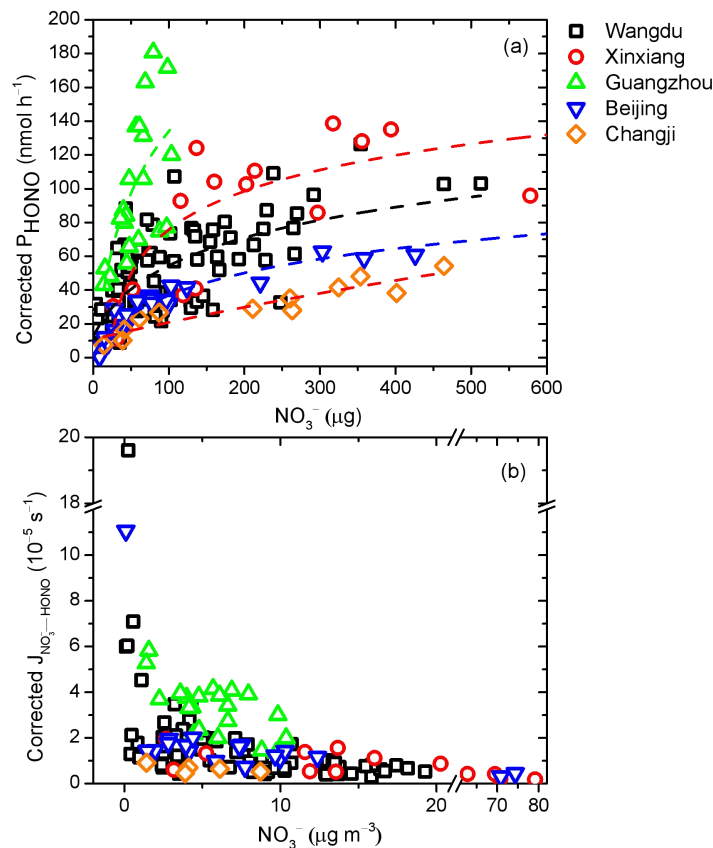
Figure 6. Relationships between (a) corrected P_{HONO} and particulate nitrate loading, and (b) corrected $J_{NO_3^- - HONO}$ and particulate nitrate concentration in different sampling locations. The dash lines in (a) were the best fits to the data for the fitting equation: the aerosol samples in Guangzhou (a=4.30, b=0.06, c=1 × 10^{-6}, R^2= 0.42), Wangdu (a=2.54, b=0.11, c=1 × 10^{-6}, R^2=0.50), Beijing (a=1.51, b=0.06, c=1×10^{-6}, R^2=0.91), Xinxiang (a=2.28, b=0.06, c=1×10^{-6}, R^2=0.47), and Changji (a=0.58, b=0.04, c=1×10^{-6}, R^2=0.86).

As shown in Figure 6, after considering the shadowing effect, the corrected P_{HONO} generally increased along with the increased amount of particulate nitrate (pNO$_3^-$, μg), but still gradually slowed down at high particulate nitrate loading, resulting in a rapid decrease in $J_{NO_3^- - HONO}$. For example, when NO$_3^-$ concentration was at low level (around 0.5 μg m^{-3}) in Wangdu, the value of corrected $J_{NO_3^- - HONO}$ was about 30 times higher than that at high NO$_3^-$ concentration (around 20 μg m^{-3}). Previous works found that the particulate nitrate was associated with matrix components in aerosol samples, and the photolysis reactivity of particulate nitrate was closely associated with the surface catalysis effect (Ye et al., 2017). In such a mechanism, the interaction between particulate nitrate and the substrate can distort the molecular structure of nitrate and increase the absorption cross-section. The increases of P_{HONO} with pNO$_3^-$ exposed to the light radiation can be fitted by a logarithm curve under different

315 environment: $P_{HONO} = \frac{a}{b}\ln(1 + b(pNO_3^-)) + c(pNO_3^-)$ (Ye et al., 2017; Ye et al., 2019). Based on this

316 fitting equation, the corrected P_{HONO} as a function of pNO_3^- was showed in Figure 6a. Interestingly,

317 these relationships under different sampling locations showed distinct upward trends. Ye et al. (2019)

318 found that this ratio of a to b was related to the catalysis power of surface reactive sites and the organic

319 matters in the matrix. The much higher ratio of a (4.30) to b (0.06) values fitted for Guangzhou than

320 those for other cities, especially Changji (a=0.58, b=0.04), suggested extra catalytic power of organic

321 components in addition to the surface reactive site on particulate nitrate. The large deviation of the ratio

322 of a to b among these cities indicated the limitation of predicting P_{HONO} only based on the relationship

323 with particulate nitrate in different atmospheric environments, and other varied aerosol chemical and

324 physical conditions should be considered as well.

325 **3.3.2 Organic matter**

326   Organic matter was ubiquitous in the atmosphere and contributed significantly to the total aerosol

327 mass. The selectivity of organic matter that coexisted in the aerosols was very important for the

328 production of HONO from the photolysis of particulate nitrate (Bao et al., 2018; Ye et al., 2016a;

329 Svoboda et al., 2013; Reeser et al., 2013; Stemmler et al., 2006; Yang et al., 2018; Beine et al., 2006;

330 Wang et al., 2021). As shown in Figure 7a, corrected P_{HONO} generally increased as the amount of OC in

331 aerosol samples (pOC, μg) went up, while these positive correlations between P_{HONO} and pOC shown

332 may be due to the moderate correlation between pNO_3^- and pOC (R^2=0.39, Figure S3). To eliminate

333 the contribution from particulate nitrate, the dependence of $J_{NO_3^- - HONO}$ on the ratio of OC to NO_3^-

334 (OC/NO_3^-) was examined:

335 Corrected $J_{NO_3^- - HONO}$=0.74×(OC/NO_3^-)+0.08   (6)

336

337
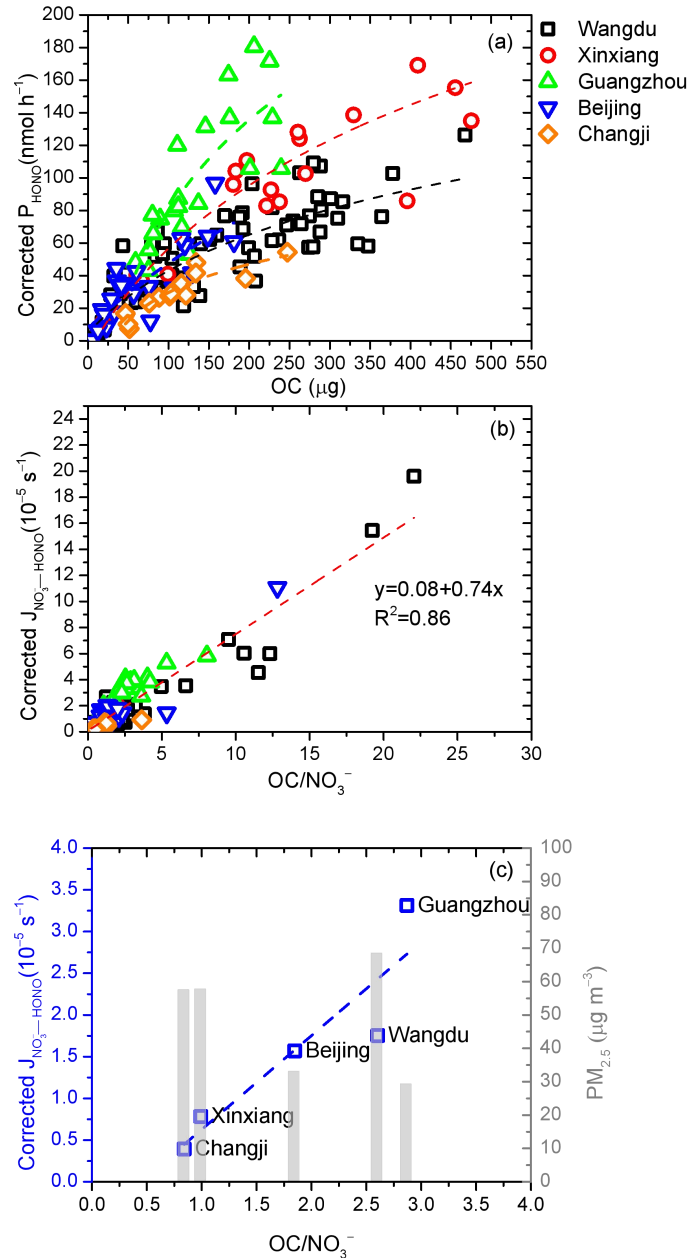
Figure 7. Relationship between (a) corrected P_{HONO} and OC loadings, (b) corrected $J_{NO_3^- - HONO}$ and

OC/NO_3^-, and (c) average corrected $J_{NO_3^- - HONO}$, $PM_{2.5}$, and OC/NO_3^- during the sampling period in

five representative cities.

As shown in Figure 7b, significant linear correlation between corrected $J_{NO_3^- - HONO}$ and OC/NO_3^-

was found, with an R^2 of 0.86. In general, high corrected $J_{NO_3^- - HONO}$ values were mostly associated

with high OC/NO_3^- ratios for aerosol samples collected in the clean areas, such as Guangzhou, where

the averaged $PM_{2.5}$ level was the lowest (Figure 7c). Low corrected $J_{NO_3^- - HONO}$ values were mostly

associated with low OC/NO_3^- ratio. Generally, cities with higher $PM_{2.5}$ levels have lower OC/NO_3^-

ratios, such as Changji and Xinxiang, however, there was an exception—Wangdu, a rural site in the

347 North China Plain, where the $PM_{2.5}$ was high but dominated by OM mainly due to local residential coal

348 combustion (Liu et al., 2016; Li et al., 2024; Liu et al., 2017). As shown in Figure 5b, the OC/NO_3^-

349 ratio in clean days was generally higher than that in polluted conditions. Interestingly, different from

350 other cities, the OC/NO_3^- ratio in Guangzhou increased at polluted conditions, which was consistent

351 with the correspondingly higher corrected $J_{NO_3^- - HONO}$ value. Guangzhou was located in the PRD

352 region, and was characterized by large fractions of OM in $PM_{2.5}$ due to large emission of VOCs from

353 numerous manufacturing industries and transport-related sources (Zheng et al., 2009), and the

354 water-soluble organic carbon (WSOC) was the dominated component in the organic aerosols

355 (WSOC/OC=0.63) (Chang et al., 2019). It's reported that organic compounds on the surface may act as

356 photosensitizers in the photolysis of particulate nitrate (Gen et al., 2022; Handley et al., 2007; Cao et

357 al., 2022; Wang et al., 2021). The association of particulate nitrate with organic matter may distort its

358 molecular structure and enhance the absorption cross section, resulting in significantly enhancement in

359 the photochemical production of HONO. The organic matter can also become hydrogen donors, and

360 directly transfer hydrogen from organic H-donors to NO_2 to form HONO (Gen et al., 2022). Therefore,

361 we suggested that the gradually increasing role of organic matter in $PM_{2.5}$ in China should be of great

362 concern.

363 **3.3.3 Other factors**

364   The acidic proton may play an important role in the photochemical production of HONO

365 and affect the release of photolysis products (Bao et al., 2018; Scharko et al., 2014). Scharko et al.

366 (2014) found that gaseous HONO production from nitrate photolysis was the highest at the lowest

367 aerosol acidity (pH, ~2) and decreased with pH, and reached almost zero at pH higher than 4. In this

368 work, the estimated pH of these aerosol samples was in the range of 1.83−3.46 (the Extended Aerosol

369 Inorganic Model, E-AIM (Shi et al., 2021; Wexler and Clegg, 2002; Clegg et al., 1998)) with detailed

370 information provided in the Supporting Information. As shown in Figure S4, however, the correlation

371 between pH and $J_{NO_3^- - HONO}$ was weak, which indicated that pH was an important factor, but not the

372 key one driving the spatial differences of $J_{NO_3^- - HONO}$ in this work. Noting that halide ions, such as

373 chlorine (Cl^-), may lead to enhancement of surface nitrate anion and promote nitrate photolysis (Gen et

374 al., 2022; Zhang et al., 2020a), we also plotted $J_{NO_3^- - HONO}$ against the molar ratio of Cl^- to NO_3^-

375 (Cl^-/NO_3^-) in Figure 8a. Even though Guangzhou was a southern coastal city, the sampling site in this

376 work was far away from the South China Sea (>50 km). Besides, during the observation period, the

377 aerosol collected in Guangzhou was more representative of inland aerosol instead of marine aerosol,

378 with the air parcel usually coming from inland directions (Figure 8b) and the ratio of Cl^- to NO_3^- (0.02)

379 much lower than that in fresh sea spray aerosol (>1.0) (Xiao et al., 2017; Pipalatkar et al., 2014; Atzei

380 et al., 2019; Wang et al., 2019). Therefore, we suggested that the halide ions were not the determining

381 factor for the high $J_{NO_3^- - HONO}$ value in Guangzhou, and the exact role of halide ions in HONO

382 formation through the photolysis of particulate nitrate required further investigation.

383

384

385
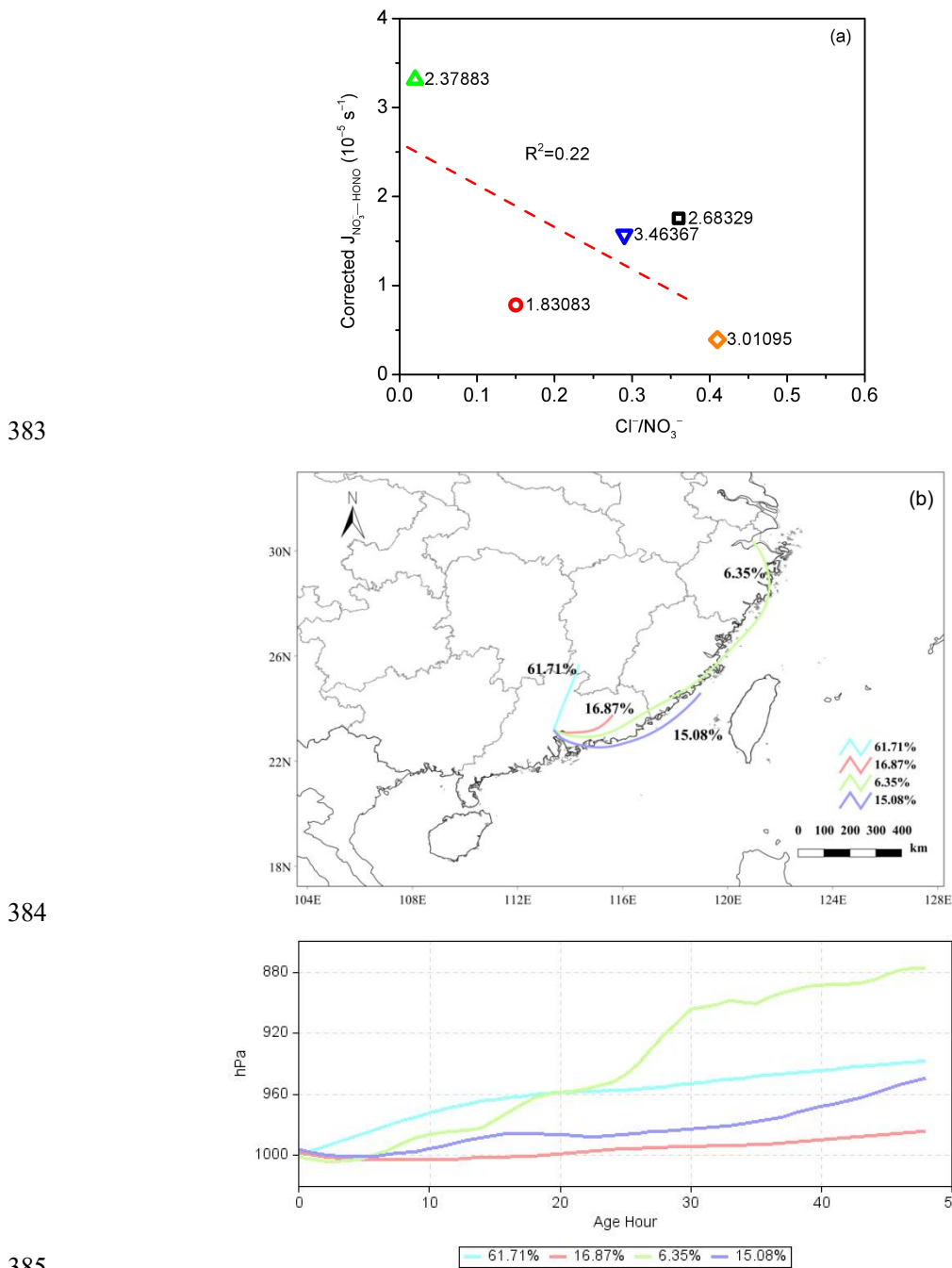
386 **Figure 8.** (a) Relationship between the average corrected $J_{NO_3^- - HONO}$ and Cl^-/NO_3^- under different

387   sampling locations, and (b) the back trajectory cluster analysis in Guangzhou during the sampling

388   period.

389   **3.4 Environmental implication**

390   The determined $J_{NO_3^- - HONO}$ was closely associated with the aerosol chemical and physical

391   characteristics, especially the coexisted organic components, and distributed around the curve as

392   expressed by Eq. (6). It's the first effort to explore the photolysis of particulate nitrate in aerosol

393   samples collected from different typical regions of China. The enhanced formation of HONO from the

394   photolysis of particulate nitrate can contribute significantly to the atmospheric oxidation capacity. To

395   assess the photolysis of particulate nitrate as a HONO daytime source, the noontime source strength of

396   HONO (S_{HONO}) through this mechanism in the air column within the planetary boundary layer can be

397   calculated by the following equation (Ye et al., 2017):

398    $S_{HONO}\ (10^{-5}\ \text{mol h}^{-1}\text{m}^{-2}) = 0.67 \times NO_3^-(\mu\text{mol m}^{-3}) \times 10^{-6} \times J_{NO_3^- - HONO} \times BLH \times 3600$ (7)

399   or

400    $S_{HONO}\ (\text{ppbv h}^{-1}) = 0.67 \times NO_3^-(\text{ppbv}) \times J_{NO_3^- - HONO} \times 3600$ (8)

401   where BLH means the boundary mixing height (m). Here, we assumed a typical BLH of 1000 m.

402   Based on the daily measured NO_3^- and corrected $J_{NO_3^- - HONO}$ value in each city, the S_{HONO} derived from

403   Eq. (7) or (8) during the observation period was showed in Table 1. It was found that, even though the

404    $J_{NO_3^- - HONO}$ in polluted days was much lower than that in clean days, due to the apparent higher NO_3^-

405   concentration, the corresponding S_{HONO} was about twice the average in clean days. The calculated

406   S_{HONO} ranged from 0.03×10^{-5} mol h^{-1} m^{-2} to 0.88×10^{-5} mol h^{-1} m^{-2} (0.01 ppbv h^{-1}–0.2 ppbv h^{-1}), with

407   the mean value of 0.36×10^{-5} mol h^{-1}m^{-2} (0.08 ppbv h^{-1}), which was comparable or higher than other

408   HONO sources (Bhattarai et al., 2019; Wang et al., 2023b; Ye et al., 2017). For example, the soil

409   HONO emission flux was measured in the range of 1.81×10^{-6} mol h^{-1} m^{-2}–4.55×10^{-6} mol h^{-1} m^{-2} in

410   the soil without suffering nitrogen fertilizer (Bhattarai et al., 2019). The mean value of S_{HONO} during

411   the observation period was the highest in Wangdu (0.42×10^{-5} mol h^{-1}m^{-2}, 0.10 ppbv h^{-1}) and

412   Guangzhou (0.41×10^{-5} mol h^{-1}m^{-2}, 0.09 ppbv h^{-1}), followed by Xinxiang (0.35×10^{-5} mol h^{-1}m^{-2}, 0.08

413   ppbv h^{-1}), Beijing (0.22×10^{-5} mol h^{-1}m^{-2}, 0.05 ppbv h^{-1}), and Changji (0.13×10^{-5} mol h^{-1}m^{-2}, 0.03

414   ppbv h^{-1}). Even though the PM$_{2.5}$ and NO_3^- concentration was the lowest in Guangzhou, the S_{HONO} was

415   much higher than other cities with air pollution. It should be noted that the S_{HONO} calculated with the

416   daily changed NO_3^- and $J_{NO_3^--HONO}$ value in this work was much lower than the value reported by Bao

417   et al. (2018) (0.78 ppbv h^{-1}), which applied the average NO_3^- (6.64 $\mu g \ m^{-3}$, 2.62 ppbv) and the

418    $J_{NO_3^--HONO}$ range (1.22×10^{-5} s^{-1}−4.84×10^{-4} s^{-1}) to simulate S_{HONO} (0.12 ppbv h^{-1}−4.57 ppbv h^{-1}). Other

419   works, such as Fu et al. (2019) and Gu et al. (2022a), applied the mean value of $J_{NO_3^--HONO}$ (8.3×10^{-5}

420   s^{-1}) and the observed NO_3^- concentration to calculate S_{HONO}. However, due to the significant decrease

421   of $J_{NO_3^--HONO}$ along with the increase of NO_3^-, the S_{HONO} calculated with mean NO_3^- or $J_{NO_3^--HONO}$

422   will be largely overestimated, thus directly influencing the identification of HONO sources. For

423   example, $J_{NO_3^--HONO}$ was the highest in Wangdu in November 23, 2023 with the value of 19.6×10^{-5} s^{-1},

424   while the corresponding NO_3^- concentration was low (0.39 $\mu g \ m^{-3}$). If applying the average NO_3^-

425   concentration (12.53 $\mu g \ m^{-3}$, equivalent to 4.53 ppbv) and the maximum $J_{NO_3^--HONO}$ value, the

426   determined S_{HONO} value would be 9.56×10^{-5} mol h^{-1} m^{-2} (2.14 ppbv h^{-1}), which was about 30 times

427   higher than the actual result (0.07 ppbv h^{-1}). Therefore, we suggested to estimate S_{HONO} with the

428   observed concentration of NO_3^- and the $J_{NO_3^--HONO}$ value derived from the parameterization equation

429   with OC/NO_3^-, thereby reducing the large uncertainties and improving estimations of HONO budget.
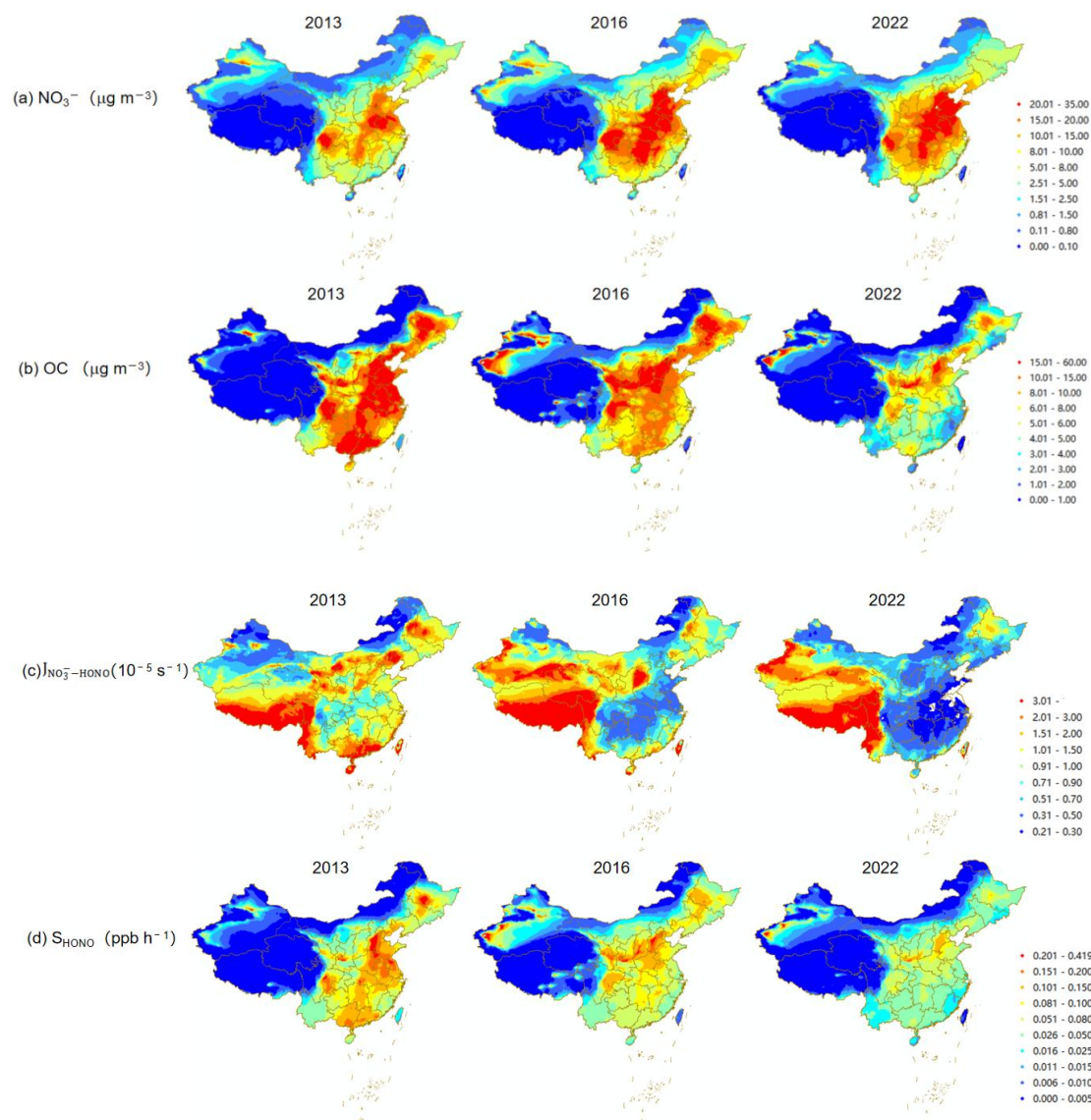
Figure 9. Spatial distributions of the daily average (a) NO_3^-, (b) OC, (c) $J_{NO_3^- - HONO}$, and (d) S_{HONO} from November 15 to December 15 in the year of 2013, 2016, and 2022 in China. The daily average concentrations of NO_3^- and OC were extracted from the Chinese high resolution $PM_{2.5}$ Component simulation concentration dataset (Kong, et al., 2024). The $J_{NO_3^- - HONO}$ and S_{HONO} estimated in this work were derived under the same environmental conditions (RH=65 %, temperature=20 °C, and light intensity=150 kW m^{-2}), thus were more representative of the potential of HONO production rather than the actual value in the real ambient environment.

On the basis of the daily average concentrations of NO_3^- and OC extracted from the Chinese high resolution $PM_{2.5}$ Component simulation concentration dataset (CAQRA-aerosol, https://www.capdatabase.cn, 15 km×15 km) (Kong, et al., 2024), the $J_{NO_3^- - HONO}$ and S_{HONO} can be estimated by Eq. (6) and (8), respectively. As shown in Figure 9, significant spatio-temporal change

characteristics of NO_3^-, OC, $J_{NO_3^--HONO}$ and S_{HONO} were demonstrated in autumn-winter seasons from 2013 to 2022 in China. The high $J_{NO_3^--HONO}$ were concentrated in the 'clean' environments (e.g., Tibetan Plateau area, South Xinjiang Basin, Yunnan-Guizhou plateaus, and Sichuan basins) and followed by those air polluted regions (e.g., NCP, Fenhe-Weihe Basin, Northeastern China, and PRD). From 2013 to 2022, with OC decreasing significantly, while NO_3^- keeping stable or even increasing, $J_{NO_3^--HONO}$ showed a downward trend in most regions. Although the $J_{NO_3^--HONO}$ in polluted regions was comparatively lower than that in 'clean' environments, the higher values of S_{HONO} were mostly distributed in these polluted regions resulting from the much higher NO_3^- concentration. However, it should be noted that the photolysis of particulate nitrate contributed only a small fraction to the needed daytime HONO source in these polluted regions, such as $1.26-3.82$ ppbv h^{-1} in the cities in the North China Plain (Hou et al., 2016; Wang et al., 2017; Lian et al., 2022; Li et al., 2018), 0.75 ppbv h^{-1} in the Western China (Huang et al., 2017), and $0.77-4.90$ ppbv h^{-1} in Southern China (Li et al., 2012; Su et al., 2008). We noted that uncertainties still exist in our simulations. Given the paucity of filed measurements of HONO production from aerosol samples in 'clean' environments, the deviation of $J_{NO_3^--HONO}$ derived from the parametrization in this work may be large in these regions. Additionally, the concentrations of NO_3^- and OC extracted from the CAQRA-aerosol in 'clean' environments were around the mean deviation level. Therefore, more field observations and simulation experiments should be taken in these 'clean' regions in the future, to enrich and improve the parametric equations of $J_{NO_3^--HONO}$, and further evaluate the contribution of nitrate photolysis to the formation of HONO in different regions in China.

4 Conclusions

This study for the first time systematically analyzed the production of HONO from the photolysis of particulate nitrate in PM$_{2.5}$ samples from multiple sites across China, shedding light to the contribution of this photolysis process to HONO daytime source in different environments. A total of 20 pairs of comparative photochemical experiments were conducted in Wangdu to evaluate and quantify the shadowing effect. We found that the corrected $J_{NO_3^--HONO}$ values varied with sampling periods and locations over a wide range, distributing from 0.16×10^{-5} s^{-1} to 19.60×10^{-5} s^{-1}. The coexisted organic components in PM$_{2.5}$ can promote the photolysis of particulate nitrate, with higher

$J_{NO_3^- - HONO}$ generally associated with higher OC/NO$_3^-$ ratio. Considering the logarithmical decrease of $J_{NO_3^- - HONO}$ with increased NO$_3^-$, we suggested that the S_{HONO} should be calculated with $J_{NO_3^- - HONO}$ derived from the parameterization equation with OC/NO$_3^-$ instead of the average value. The photolysis of particulate nitrate can become a potential daytime HONO source in southern urban cities, such as GuangZ, which was characterized by large VOCs emissions and enhanced formation of secondary particulate organic matter. Our work has provided an important reference for the research in other areas in the world with high proportion of organic components in aerosol samples, such as United States (Hass-Mitchell et al., 2024) and Europe (Bressi et al., 2021). To note, the filter samples collected in this work may not cover all representative environments in China, especially the background sites, more field observations and simulation experiments are needed in the future to better constrain the parameterization and mechanism of particulate nitrate photolysis.

482   **Data availability.** The data used in this paper can be provided upon request from the corresponding

483   author.

484

485   **Author contributions. J W, B L and K Z** conceived the study and designed the experiments. **J W, B**

486   **L, J G, C C, L W, Y Z, J L, Y Z, and X D** analyzed the data. **J W and B L** prepared the manuscript

487   and all the coauthors helped improve the manuscript.

488

489   **Competing interests.** The authors declare that they have no conflict of interest.

490

491   **Acknowledgement.** We thank the Data Integration Program of the Major Research Plan of the

492   National Natural Science Foundation of China (No. 92044303, https://www.capdatabase.cn) for

493   making the high-resolution simulation dataset of $PM_{2.5}$ chemical composition in Chinese from 2013 to

494   2020 available.

495

496   **Financial support.** This work was supported by the Central Level, Scientific Research Institutes for

497   Basic R&D Special Fund Business, China (No. 2022YSKY-26), and the National Key Research and

498   Development Program of China (No. 2022YFC3701100).

499   **References**

500   Ammann, M., Kalberer, M., Jost, D. T., Tobler, L., Rössler, E., Piguet, D., Gäggeler, H. W., and

501   Baltensperger, U.: Heterogeneous production of nitrous acid on soot in polluted air masses, Nature,

502   395, 157-160, 10.1038/25965, 1998.

503   Andersen, S. T., Carpenter, L. J., Reed, C., Lee, J. D., Chance, R., Sherwen, T., Vaughan, A. R., Stewart,

504   J., Edwards, P. M., Bloss, W. J., Sommariva, R., Crilley, L. R., Nott, G. J., Neves, L., Read, K.,

505   Heard, D. E., Seakins, P. W., Whalley, L. K., Boustead, G. A., Fleming, L. T., Stone, D., and Fomba,

506   K. W.: Extensive field evidence for the release of HONO from the photolysis of nitrate aerosols, Sci.

507   Adv., 9, eadd6266, doi:10.1126/sciadv.add6266, 2023.

508   Atzei, D., Fermo, P., Vecchi, R., Fantauzzi, M., Comite, V., Valli, G., Cocco, F., and Rossi, A.:

509   Composition and origin of $PM_{2.5}$ in Mediterranean Countryside, Environ. Pollut., 246, 294-302,

510   https://doi.org/10.1016/j.envpol.2018.12.012, 2019.

511   Bao, F., Li, M., Zhang, Y., Chen, C., and Zhao, J.: Photochemical aging of Beijing urban $PM_{2.5}$: HONO

512   production, Environ. Sci. Technol., 52, 6309-6316, 10.1021/acs.est.8b00538, 2018.

513   Bao, F., Jiang, H., Zhang, Y., Li, M., Ye, C., Wang, W., Ge, M., Chen, C., and Zhao, J.: The key role of

514   sulfate in the photochemical renoxification on real $PM_{2.5}$, Environ. Sci. Technol., 54, 3121-3128,

515   10.1021/acs.est.9b06764, 2020.

516   Beine, H. J., Amoroso, A., Dominé, F., King, M. D., Nardino, M., Ianniello, A., and France, J. L.:

517   Surprisingly small HONO emissions from snow surfaces at Browning Pass, Antarctica, Atmos.

518   Chem. Phys., 6, 2569-2580, 10.5194/acp-6-2569-2006, 2006.

519   Bhattarai, H. R., Liimatainen, M., Nykänen, H., Kivimäenpää, M., Martikainen, P. J., and Maljanen, M.:

520   Germinating wheat promotes the emission of atmospherically significant nitrous acid (HONO) gas

521   from soils, Soil Biol. Biochem., 136, 10.1016/j.soilbio.2019.06.014, 2019.

522   Bressi, M., Cavalli, F., Putaud, J. P., Fröhlich, R., Petit, J. E., Aas, W., Äijälä, M., Alastuey, A., Allan, J.

523   D., Aurela, M., Berico, M., Bougiatioti, A., Bukowiecki, N., Canonaco, F., Crenn, V., Dusanter, S.,

524   Ehn, M., Elsasser, M., Flentje, H., Graf, P., Green, D. C., Heikkinen, L., Hermann, H., Holzinger, R.,

525   Hueglin, C., Keernik, H., Kiendler-Scharr, A., Kubelová, L., Lunder, C., Maasikmets, M., Makeš, O.,

526   Malaguti, A., Mihalopoulos, N., Nicolas, J. B., O'Dowd, C., Ovadnevaite, J., Petralia, E., Poulain, L.,

527   Priestman, M., Riffault, V., Ripoll, A., Schlag, P., Schwarz, J., Sciare, J., Slowik, J., Sosedova, Y.,

Stavroulas, I., Teinemaa, E., Via, M., Vodička, P., Williams, P. I., Wiedensohler, A., Young, D. E., Zhang, S., Favez, O., Minguillón, M. C., and Prevot, A. S. H.: A European aerosol phenomenology - 7: High-time resolution chemical characteristics of submicron particulate matter across Europe, Atmos. Environ.: X, 10, 10.1016/j.aeaoa.2021.100108, 2021.

Cao, Y., Ma, Q., Chu, B., and He, H.: Homogeneous and heterogeneous photolysis of nitrate in the atmosphere: state of the science, current research needs, and future prospects, Front. Env. Sci. Eng., 17, 10.1007/s11783-023-1648-6, 2022.

Chang, D., Wang, Z., Guo, J., Li, T., Liang, Y., Kang, L., Xia, M., Wang, Y., Yu, C., Yun, H., Yue, D., and Wang, T.: Characterization of organic aerosols and their precursors in southern China during a severe haze episode in January 2017, Sci. Total. Environ., 691, 101-111, 10.1016/j.scitotenv.2019.07.123, 2019.

Cheng, C., Yang, S., Yuan, B., Pei, C., Zhou, Z., Mao, L., Liu, S., Chen, D., Cheng, X., Li, M., Shao, M., and Zhou, Z.: The significant contribution of nitrate to a severe haze event in the winter of Guangzhou, China, Sci. Total. Environ., 909, 168582, 10.1016/j.scitotenv.2023.168582, 2024.

Clegg, S. L., Brimblecombe, P., and Wexler, A. S.: Thermodynamic Model of the System $H^+-NH_4^+-Na^+-SO_4^{2-}-NO_3^--Cl^--H_2O$ at 298.15 K, J. Phy. Chem. A, 102, 2155-2171, 10.1021/jp973043j, 1998.

Finlayson-Pitts, B. J. a. P. J., J. N.: Chemistry of the upper and lower atmosphere: theory, experiments, and applications, Academic Press, San Diego, CA, xxii+969 pp., ISBN 0-12-257060-x, 2000.

Fu, X., Wang, T., Zhang, L., Li, Q., Wang, Z., Xia, M., Yun, H., Wang, W., Yu, C., Yue, D., Zhou, Y., Zheng, J., and Han, R.: The significant contribution of HONO to secondary pollutants during a severe winter pollution event in southern China, Atmos. Chem. Phys., 19, 1-14, 10.5194/acp-19-1-2019, 2019.

Gelencsér, A., Hoffer, A., Kiss, G., Tombácz, E., Kurdi, R., and Bencze, L.: In-situ formation of light-absorbing organic matter in cloud water, J. Atmos. Chem., 45, 25-33, 10.1023/A:1024060428172, 2003.

Gen, M., Liang, Z., Zhang, R., Go Mabato, B. R., and Chan, C. K.: Particulate nitrate photolysis in the atmosphere, Environ. Sci.-Atmos., 2, 111-127, 10.1039/d1ea00087j, 2022.

Gu, R., Shen, H., Xue, L., Wang, T., Gao, J., Li, H., Liang, Y., Xia, M., Yu, C., Liu, Y., and Wang, W.: Investigating the sources of atmospheric nitrous acid (HONO) in the megacity of Beijing, China, Sci.

558   Total Environ., 812, 10.1016/j.scitotenv.2021.152270, 2022a.

559   Gu, R., Wang, W., Peng, X., Xia, M., Zhao, M., Zhang, Y., Wang, Y., Liu, Y., Shen, H., Xue, L., Wang,

560   T., and Wang, W.: Nitrous acid in the polluted coastal atmosphere of the South China Sea: Ship

561   emissions, budgets, and impacts, Sci. Total. Environ., 153692, 10.1016/j.scitotenv.2022.153692,

562   2022b.

563   Handley, S. R., Clifford, D., and Donaldson, D. J.: Photochemical loss of nitric acid on organic films: a

564   possible recycling mechanism for NOx, Environ. Sci. Technol., 41, 3898-3903, 10.1021/es062044z,

565   2007.

566   Hass-Mitchell, T., Joo, T., Rogers, M., Nault, B. A., Soong, C., Tran, M., Seo, M., Machesky, J. E.,

567   Canagaratna, M., Roscioli, J., Claflin, M. S., Lerner, B. M., Blomdahl, D. C., Misztal, P. K., Ng, N.

568   L., Dillner, A. M., Bahreini, R., Russell, A., Krechmer, J. E., Lambe, A., and Gentner, D. R.:

569   Increasing contributions of temperature-dependent oxygenated organic aerosol to summertime

570   particulate matter in New York City, ACS Environ. Sci. Technol. Air, 1, 113-128,

571   10.1021/acsestair.3c00037, 2024.

572   Hou, S., Tong, S., Ge, M., and An, J.: Comparison of atmospheric nitrous acid during severe haze and

573   clean periods in Beijing, China, Atmos. Environ., 124, 199-206, 10.1016/j.atmosenv.2015.06.023,

574   2016.

575   Huang, R.., Yang, L., Cao, J., Wang, Q., Tie, X., Ho, K., Shen, Z., Zhang, R., Li, G., Zhu, C., Zhang, N.,

576   Dai, W., Zhou, J., Liu, S., Chen, Y., Chen, J., and O'Dowd, C. D.: Concentration and sources of

577   atmospheric nitrous acid (HONO) at an urban site in Western China, Sci. Total Environ., 593-594,

578   165-172, https://doi.org/10.1016/j.scitotenv.2017.02.166, 2017.

579   Kim, M. and Or, D.: Microscale pH variations during drying of soils and desert biocrusts affect HONO

580   and NH_3 emissions, Nat. Commun., 10, 3944, 10.1038/s41467-019-11956-6, 2019.

581   Kong, L., Tang, X., Zhu, J., Wang, Z., Liu, B., Zhu, Y., Zhu, L., Chen, D., Hu, K., Wu, H., Wu, Q.,

582   Shen, J., Sun, Y., Liu, Z., Xin, J., Ji, D., and Zheng, M.: High-resolution simulation dataset of hourly

583    $PM_{2.5}$ chemical composition in China (CAQRA-aerosol) from 2013 to 2020, Adv. Atmos. Sci., 41,

584   1-16, 10.1007/s00376-024-4046-5, 2024.

585   Kurtenbach, R., Becker, K. H., Gomes, J. A. G., Kleffmann, J., Lörzer, J. C., Spittler, M., Wiesen, P.,

586   Ackermann, R., Geyer, A., and Platt, U.: Investigations of emissions and heterogeneous formation of

587   HONO   in   a   road   traffic   tunnel,   Atmos.   Environ.,   35,   3385-3394,

588   https://doi.org/10.1016/S1352-2310(01)00138-8, 2001.

589   Lee, J. D., Whalley, L. K., Heard, D. E., Stone, D., Dunmore, R. E., Hamilton, J. F., Young, D. E.,

590   Allan, J. D., Laufs, S., and Kleffmann, J.: Detailed budget analysis of HONO in central London

591   reveals a missing daytime source, Atmos. Chem. Phys., 16, 2747-2764, 10.5194/acp-16-2747-2016,

592   2016.

593   Li, D., Xue, L., Wen, L., Wang, X., Chen, T., Mellouki, A., Chen, J., and Wang, W.: Characteristics and

594   sources of nitrous acid in an urban atmosphere of northern China: Results from 1-yr continuous

595   observations, Atmos. Environ., 182, 296-306, https://doi.org/10.1016/j.atmosenv.2018.03.033, 2018.

596   Li, W., Tong, S., Cao, J., Su, H., Zhang, W., Wang, L., Jia, C., Zhang, X., Wang, Z., Chen, M., and Ge,

597   M.: Comparative observation of atmospheric nitrous acid (HONO) in Xi'an and Xianyang located in

598   the GuanZhong basin of western China, Environ. Pollut., 289, 117679,

599   10.1016/j.envpol.2021.117679, 2021.

600   Li, X., Brauers, T., Häseler, R., Bohn, B., Fuchs, H., Hofzumahaus, A., Holland, F., Lou, S., Lu, K. D.,

601   Rohrer, F., Hu, M., Zeng, L. M., Zhang, Y. H., Garland, R. M., Su, H., Nowak, A., Wiedensohler, A.,

602   Takegawa, N., Shao, M., and Wahner, A.: Exploring the atmospheric chemistry of nitrous acid

603   (HONO) at a rural site in Southern China, Atmos. Chem. Phys., 12, 1497-1513,

604   10.5194/acp-12-1497-2012, 2012.

605   Li, Y., An, J., Min, M., Zhang, W., Wang, F., and Xie, P.: Impacts of HONO sources on the air quality

606   in Beijing, Tianjin and Hebei Province of China, Atmos. Environ., 45, 4735-4744,

607   https://doi.org/10.1016/j.atmosenv.2011.04.086, 2011.

608   Li, Z., Ren, Z., Liu, C., Ning, Z., Liu, J., Liu, J., Zhai, Z., Ma, X., Chen, L., Zhang, Y., Bai, L., and

609   Kong, S.: Heterogeneous variations in wintertime $PM_{2.5}$ sources, compositions and exposure risks at

610   urban/suburban rural/remote rural areas in the post COVID-19/Clean-Heating period, Atmos.

611   Environ., 326, 120463, https://doi.org/10.1016/j.atmosenv.2024.120463, 2024.

612   Lian, C., Wang, W., Chen, Y., Zhang, Y., Zhang, J., Liu, Y., Fan, X., Li, C., Zhan, J., Lin, Z., Hua, C.,

613   Zhang, W., Liu, M., Li, J., Wang, X., An, J., and Ge, M.: Long-term winter observation of nitrous

614   acid in the urban area of Beijing, J. Environ. Sci. (China), 114, 334-342, 10.1016/j.jes.2021.09.010,

615   2022.

616   Liang, Y., Zha, Q., Wang, W., Cui, L., Lui, K. H., Ho, K. F., Wang, Z., Lee, S., and Wang, T.: Revisiting

617   nitrous acid (HONO) emission from on-road vehicles: A tunnel study with a mixed fleet, J. Air Waste

618   Manage., 67, 797-805, 10.1080/10962247.2017.1293573, 2017.

619   Liao, S., Zhang, J., Yu, F., Zhu, M., Liu, J., Ou, J., Dong, H., Sha, Q., Zhong, Z., Xie, Y., Luo, H.,

620   Zhang, L., and Zheng, J.: High gaseous nitrous acid (HONO) emissions from light-duty diesel

621   vehicles, Environ. Sci. Technol., 55, 200-208, 10.1021/acs.est.0c05599, 2021.

622   Liu, P., Zhang, C., Mu, Y., Liu, C., Xue, C., Ye, C., Liu, J., Zhang, Y., and Zhang, H.: The possible

623   contribution of the periodic emissions from farmers' activities in the North China Plain to

624   atmospheric water-soluble ions in Beijing, Atmos. Chem. Phys., 16, 10097-10109,

625   10.5194/acp-16-10097-2016, 2016.

626   Liu, P., Zhang, C., Xue, C., Mu, Y., Liu, J., Zhang, Y., Tian, D., Ye, C., Zhang, H., and Guan, J.: The

627   contribution of residential coal combustion to atmospheric $PM_{2.5}$ in northern China during winter,

628   Atmos. Chem. Phys., 17, 11503-11520, 10.5194/acp-17-11503-2017, 2017.

629   Liu, Y., Lu, K., Li, X., Dong, H., Tan, Z., Wang, H., Zou, Q., Wu, Y., Zeng, L., Hu, M., Min, K.-E.,

630   Kecorius, S., Wiedensohler, A., and Zhang, Y.: A comprehensive model test of the HONO sources

631   constrained to field measurements at rural North China Plain, Environ. Sci. Technol., 53, 3517-3525,

632   10.1021/acs.est.8b06367, 2019.

633   Melissa A, D.: Soil surface acidity plays a determining role in the atmospheric-terrestrial exchange of

634   nitrous acid, Proc. Natl. Acad. Sci. U. S. A., 52, 18472-18477, 10.1073/pnas.1418545112, 2014.

635   Monge, M. E., D'Anna, B., Mazri, L., Giroir-Fendler, A., Ammann, M., Donaldson, D. J., and George,

636   C.: Light changes the atmospheric reactivity of soot, Proc. Natl. Acad. Sci. U. S. A., 107, 6605-6609,

637   10.1073/pnas.0908341107, 2010.

638   Mora Garcia, S. L., Pandit, S., Navea, J. G., and Grassian, V. H.: Nitrous acid (HONO) formation from

639   the irradiation of aqueous nitrate solutions in the presence of marine chromophoric dissolved organic

640   matter: comparison to other organic photosensitizers, ACS Earth Space Chem., 5, 3056-3064,

641   10.1021/acsearthspacechem.1c00292, 2021.

642   Oswald, R., Behrendt, T., Ermel, M., Wu, D., Su, H., Cheng, Y., Breuninger, C., Moravek, A., Mougin,

643   E., Delon, C., Loubet, B., Pommerening-Roser, A., Sorgel, M., Poschl, U., Hoffmann, T., Andreae,

644   M. O., Meixner, F. X., and Trebs, I.: HONO emissions from soil bacteria as a major source of

645   atmospheric reactive nitrogen, Science, 341, 1233-1235, 10.1126/science.1242266, 2013.

646   Pipalatkar, P., Khaparde, V. V., Gajghate, D. G., and Bawase, M. A.: Source apportionment of $PM_{2.5}$

647   using a CMB model for a centrally located Indian city, Aerosol Air Qual. Res., 14, 1089-1099,

648   10.4209/aaqr.2013.04.0130, 2014.

649   Reeser, D. I., Kwamena, N.-O. A., and Donaldson, D. J.: Effect of organic coatings on gas-phase

650   nitrogen dioxide production from aqueous nitrate photolysis, J. Phys. Chem. C, 117, 22260-22267,

651   10.1021/jp401545k, 2013.

652   Ren, X., Harder, H., Martinez, M., Lesher, R. L., Oliger, A., Simpas, J. B., Brune, W. H., Schwab, J. J.,

653   Demerjian, K. L., He, Y., Zhou, X., and Gao, H.: OH and HO_2 Chemistry in the urban atmosphere of

654   New York City, Atmos. Environ., 37, 3639-3651, https://doi.org/10.1016/S1352-2310(03)00459-X,

655   2003.

656   Romer, P. S., Wooldridge, P. J., Crounse, J. D., Kim, M. J., Wennberg, P. O., Dibb, J. E., Scheuer, E.,

657   Blake, D. R., Meinardi, S., Brosius, A. L., Thames, A. B., Miller, D. O., Brune, W. H., Hall, S. R.,

658   Ryerson, T. B., and Cohen, R. C.: Constraints on aerosol nitrate photolysis as a potential source of

659   HONO and NOx, Environ. Sci. Technol., 52, 13738-13746, 10.1021/acs.est.8b03861, 2018.

660   Scharko, N. K., Berke, A. E., and Raff, J. D.: Release of nitrous acid and nitrogen dioxide from nitrate

661   photolysis in acidic aqueous solutions, Environ. Sci. Technol., 48, 11991-12001, 10.1021/es503088x,

662   2014.

663   Shi, Q., Tao, Y., Krechmer, J. E., Heald, C. L., Murphy, J. G., Kroll, J. H., and Ye, Q.: Laboratory

664   investigation of renoxification from the photolysis of inorganic particulate nitrate, Environ. Sci.

665   Technol., 55, 854-861, 10.1021/acs.est.0c06049, 2021.

666   Slater, E. J., Whalley, L. K., Woodward-Massey, R., Ye, C., Lee, J. D., Squires, F., Hopkins, J. R.,

667   Dunmore, R. E., Shaw, M., Hamilton, J. F., Lewis, A. C., Crilley, L. R., Kramer, L., Bloss, W., Vu, T.,

668   Sun, Y., Xu, W., Yue, S., Ren, L., Acton, W. J. F., Hewitt, C. N., Wang, X., Fu, P., and Heard, D. E.:

669   Elevated levels of OH observed in haze events during wintertime in central Beijing, Atmos. Chem.

670   Phys., 20, 14847-14871, 10.5194/acp-20-14847-2020, 2020.

671   Stemmler, K., Ammann, M., Donders, C., Kleffmann, J., and George, C.: Photosensitized reduction of

672   nitrogen dioxide on humic acid as a source of nitrous acid, Nature, 440, 195-198,

673   10.1038/nature04603, 2006.

674   Su, H., Cheng, Y. F., Shao, M., Gao, D. F., Yu, Z. Y., Zeng, L. M., Slanina, J., Zhang, Y. H., and

675   Wiedensohler, A.: Nitrous acid (HONO) and its daytime sources at a rural site during the 2004

676   PRIDE-PRD experiment in China, J. Geophys. Res. Atmos., 113, 10.1029/2007jd009060, 2008.

677   Su, H., Cheng, Y., Oswald, R., Behrendt, T., Trebs, I., Meixner, F. X., Andreae, M. O., Cheng, P., Zhang,

678 Y., and Poschl, U.: Soil nitrite as a source of atmospheric HONO and OH radicals, Science, 333,

679 1616-1618, 10.1126/science.1207687, 2011.

680 Svoboda, O., Kubelová, L., and Slavíček, P.: Enabling forbidden processes: quantum and solvation

681 enhancement of nitrate anion UV absorption, J. Phys. Chem. A, 117, 12868-12877,

682 10.1021/jp4098777, 2013.

683 Villena, G., Wiesen, P., Cantrell, C. A., Flocke, F., Fried, A., Hall, S. R., Hornbrook, R. S., Knapp, D.,

684 Kosciuch, E., Mauldin, R. L., McGrath, J. A., Montzka, D., Richter, D., Ullmann, K., Walega, J.,

685 Weibring, P., Weinheimer, A., Staebler, R. M., Liao, J., Huey, L. G., and Kleffmann, J.: Nitrous acid

686 (HONO) during polar spring in Barrow, Alaska: A net source of OH radicals?, J. Geophys. Res., 116,

687 10.1029/2011jd016643, 2011.

688 Wang, H., Ding, J., Xu, J., Wen, J., Han, J., Wang, K., Shi, G., Feng, Y., Ivey, C. E., Wang, Y., Nenes,

689 A., Zhao, Q., and Russell, A. G.: Aerosols in an arid environment: The role of aerosol water content,

690 particulate acidity, precursors, and relative humidity on secondary inorganic aerosols, Sci. Total

691 Environ., 646, 564-572, https://doi.org/10.1016/j.scitotenv.2018.07.321, 2019.

692 Wang, J., Zhang, X., Guo, J., Wang, Z., and Zhang, M.: Observation of nitrous acid (HONO) in Beijing,

693 China: Seasonal variation, nocturnal formation and daytime budget, Sci. Total Environ., 587-588,

694 350-359, 10.1016/j.scitotenv.2017.02.159, 2017.

695 Wang, J., Gao, J., Che, F., Wang, Y., Lin, P., and Zhang, Y.: Decade-long trends in chemical component

696 properties of $PM_{2.5}$ in Beijing, China (2011-2020), Sci. Total Environ., 832, 154664,

697 10.1016/j.scitotenv.2022.154664, 2022a.

698 Wang, J., Gao, J., Che, F., Wang, Y., Lin, P., and Zhang, Y.: Dramatic changes in aerosol composition

699 during the 2016-2020 heating seasons in Beijing-Tianjin-Hebei region and its surrounding areas: The

700 role of primary pollutants and secondary aerosol formation, Sci. Total. Environ., 849, 157621,

701 10.1016/j.scitotenv.2022.157621, 2022b.

702 Wang, J., Zhang, Y., Zhang, C., Wang, Y., Zhou, J., Whalley, L. K., Slater, E. J., Dyson, J. E., Xu, W.,

703 Cheng, P., Han, B., Wang, L., Yu, X., Wang, Y., Woodward-Massey, R., Lin, W., Zhao, W., Zeng, L.,

704 Ma, Z., Heard, D. E., and Ye, C.: Validating HONO as an intermediate tracer of the external cycling

705 of reactive nitrogen in the background atmosphere, Environ. Sci. Technol., 57, 5474-5484,

706 10.1021/acs.est.2c06731, 2023a.

707 Wang, Y., Fu, X., Wang, T., Ma, J., Gao, H., Wang, X., and Pu, W.: Large contribution of nitrous acid to

708   soil-emitted reactive oxidized nitrogen and its effect on air quality, Environ. Sci. Technol., 57,
709   3516-3526, 10.1021/acs.est.2c07793, 2023b.

710 Wang, Y., Xiao, S., Zhang, Y., Chang, H., Martin, R. V., Van Donkelaar, A., Gaskins, A., Liu, Y., Liu, P.,
711   and Shi, L.: Long-term exposure to $PM_{2.5}$ major components and mortality in the southeastern
712   United States, Environ. Int., 158, 106969, 10.1016/j.envint.2021.106969, 2022c.

713 Wang, Y., Huang, D. D., Huang, W., Liu, B., Chen, Q., Huang, R., Gen, M., Mabato, B. R. G., Chan, C.
714   K., Li, X., Hao, T., Tan, Y., Hoi, K. I., Mok, K. M., and Li, Y. J.: Enhanced nitrite production from
715   the aqueous photolysis of nitrate in the presence of vanillic acid and implications for the roles of
716   light-absorbing organics, Environ. Sci. Technol., 55, 15694-15704, 10.1021/acs.est.1c04642, 2021.

717 Wang, Z., Zhang, D., Liu, B., Li, Y., Chen, T., Sun, F., Yang, D., Liang, Y., Chang, M., Yang, L., and
718   Lin, A.: Analysis of chemical characteristics of $PM_{2.5}$ in Beijing over a 1-year period, J. Atmos.
719   Chem., 73, 407-425, 10.1007/s10874-016-9334-8, 2016.

720 Wexler, A. S. and Clegg, S. L.: Atmospheric aerosol models for systems including the ions H^+, NH_4^+,
721   Na^+, SO_4^{2-}, NO_3^-, Cl^-, Br^-, and H_2O, J. Geophys. Res. Atmos., 107, ACH 14-1-ACH 14-14,
722   https://doi.org/10.1029/2001JD000451, 2002.

723 Xiao, H. W., Xiao, H. Y., Luo, L., Shen, C. Y., Long, A. M., Chen, L., Long, Z. H., and Li, D. N.:
724   Atmospheric aerosol compositions over the South China Sea: temporal variability and source
725   apportionment, Atmos. Chem. Phys., 17, 3199-3214, 10.5194/acp-17-3199-2017, 2017.

726 Yang, W., Han, C., Yang, H., and Xue, X.: Significant HONO formation by the photolysis of nitrates in
727   the presence of humic acids, Environ. Pollut., 243, 679-686, 10.1016/j.envpol.2018.09.039, 2018.

728 Ye, C., Gao, H., Zhang, N., and Zhou, X.: Photolysis of nitric acid and nitrate on natural and artificial
729   surfaces, Environ. Sci. Technol., 50, 3530-3536, 10.1021/acs.est.5b05032, 2016a.

730 Ye, C., Zhang, N., Gao, H., and Zhou, X.: Photolysis of particulate nitrate as a source of HONO and
731   NOx, Environ. Sci. Technol., 51, 6849-6856, 10.1021/acs.est.7b00387, 2017.

732 Ye, C., Zhang, N., Gao, H., and Zhou, X.: Matrix effect on surface-catalyzed photolysis of nitric acid,
733   Sci. Rep., 9, 4351, 10.1038/s41598-018-37973-x, 2019.

734 Ye, C., Zhou, X., Pu, D., Stutz, J., Festa, J., Spolaor, M., Tsai, C., Cantrell, C., Mauldin, R. L., Campos,
735   T., Weinheimer, A., Hornbrook, R. S., Apel, E. C., Guenther, A., Kaser, L., Yuan, B., Karl, T.,
736   Haggerty, J., Hall, S., Ullmann, K., Smith, J. N., Ortega, J., and Knote, C.: Rapid cycling of reactive
737   nitrogen in the marine boundary layer, Nature, 532, 489-491, 10.1038/nature17195, 2016b.

738 Zhang, L., Wang, T., Zhang, Q., Zheng, J., Xu, Z., and Lv, M.: Potential sources of nitrous acid (HONO) and their impacts on ozone: A WRF-Chem study in a polluted subtropical region, J. Geophys. Res. Atmos., 121, 3645-3662, https://doi.org/10.1002/2015JD024468, 2016.

741 Zhang, R., Gen, M., Huang, D., Li, Y., and Chan, C. K.: Enhanced sulfate production by nitrate photolysis in the presence of halide ions in atmospheric particles, Environ. Sci. Technol., 54, 3831-3839, 10.1021/acs.est.9b06445, 2020a.

744 Zhang, W., Tong, S., Jia, C., Wang, L., Liu, B., Tang, G., Ji, D., Hu, B., Liu, Z., Li, W., Wang, Z., Liu, Y., Wang, Y., and Ge, M.: Different HONO sources for three layers at the urban area of Beijing, Environ. Sci. Technol., 54, 12870-12880, 10.1021/acs.est.0c02146, 2020b.

747 Zheng, J., Shao, M., Che, W., Zhang, L., Zhong, L., Zhang, Y., and Streets, D.: Speciated VOC emission inventory and spatial patterns of ozone formation potential in the Pearl River Delta, China, Environ. Sci. Technol., 43, 8580-8586, 10.1021/es901688e, 2009.

750 Zhou, X., Gao, H., He, Y., Huang, G., Bertman, S. B., Civerolo, K., and Schwab, J.: Nitric acid photolysis on surfaces in low-NOx environments: Significant atmospheric implications, Geophys. Res. Let., 30, https://doi.org/10.1029/2003GL018620, 2003.

753 Zhou, X., Zhang, N., TerAvest, M., Tang, D., Hou, J., Bertman, S., Alaghmand, M., Shepson, P. B., Carroll, M. A., Griffith, S., Dusanter, S., and Stevens, P. S.: Nitric acid photolysis on forest canopy surface as a source for tropospheric nitrous acid, Nat. Geosci., 4, 440-443, 10.1038/ngeo1164, 2011.